

Report

R-24-02

February 2024



Microstructure and dislocation density analysis of P355N pressure vessel steel grade

Joacim Hagström

SVENSK KÄRNBRÄNSLEHANTERING AB

SWEDISH NUCLEAR FUEL
AND WASTE MANAGEMENT CO

Box 3091, SE-169 03 Solna
Phone +46 8 459 84 00
skb.se

SVENSK KÄRNBRÄNSLEHANTERING

ISSN 1402-3091

SKB R-24-02

ID 2032273

February 2024

Microstructure and dislocation density analysis of P355N pressure vessel steel grade

Joacim Hagström, Swerim AB

This report concerns a study which was conducted for Svensk Kärnbränslehantering AB (SKB). The conclusions and viewpoints presented in the report are those of the author. SKB may draw modified conclusions, based on additional literature sources and/or expert opinions.

This report is published on www.skb.se

© 2024 Svensk Kärnbränslehantering AB

Summary

The microstructure in large steel tubes, diameter 800 mm and wall thickness 50 mm, from P355N pressure vessel steel grade, was analysed by SEM imaging, EDS- and EBSD analysis. The microstructure was ferritic/perlitic with large ferrite grains and islands of perlite. The perlite islands showed a sub-structure with smaller ferrite sub-grains and cementite particles embedded in the structure. The perlite was not in the form of lamellas but mostly rounded cementite particles and also elongated particles in grain boundaries.

The geometrically necessary dislocation density (GND) was higher in the perlite regions where also low angle sub-grain boundaries were frequent. Sub-grains are separated by low angle grain boundaries composed of dislocations.

There appears to be no consistent differences between the different tubes and positions in the tubes (ST7/ST4). The areas with low GND ($0-9.5 \times 10^{14} \text{ m}^{-2}$) make up between 87 % and 96 % of the total area, and the variation between the samples in GND was mostly due to variations in the fraction of perlite in the analysed area. The maximum GND varied between 61.8×10^{14} and $64.4 \times 10^{14} \text{ m}^{-2}$.

An important result from this study was also that the GND in perlite areas was considerable higher compared to the ferrite areas. Additionally, the perlite contained dislocation sub-boundaries which was not present in the ferrite. This understanding will be important for future planning of dislocation density analysis with more local techniques, i.e. TEM.

Contents

1	Introduction	7
2	Investigation	9
3	Results	11
4	Conclusions	19
5	Discussion	19
6	Potential further work	19
	References	21
Appendix	Images for all materials and positions/directions	23

1 Introduction

Dislocation analysis in scanning electron microscopy (SEM) by electron backscatter diffraction (EBSD) has the ability to give an overview of the materials homogeneity in contrast to transmission electron microscopy (TEM) that gives very local information. The aim of this work was to give a good understanding of the materials microstructure and a basic analysis of its dislocation density. This was done by analysing so called geometrically necessary dislocation densities (GND) by EBSD.

EBSD analyses phases and crystal orientations at high precision and speed. The angular precision in normal analysis using Hough transformation (Electron Backscatter Diffraction 2024a.) is often reported to be better than 0.5° (Electron Backscatter Diffraction 2024b). Modern EBSD systems with improved algorithms perform even better and by using higher detector image resolution and longer exposure time it is possible to increase the precision to below 0.1° . This will however slow down the analysis significantly. Further processing of the data using pattern matching techniques have the ability to further improve the angular precision and it is possible to reach below 0.01° .

Every dislocation within the crystal lattice causes a very small change in orientation, due to the shift in the rows of atoms; although this orientation change is usually too small to be measured accurately using EBSD, the accumulated orientation change (or the curvature of the lattice) caused by many dislocations of the same sign can be measured. Dislocation analysis by EBSD is performed by comparing the misorientation angle between an analysed point and the surrounding 8 neighbouring points (Electron Backscatter Diffraction 2024c, Pantleon 2008, Konijnenberg et al. 2015, Wheeler et al. 2009). This is done for each point in the analysis and in this way it was possible to calculate the dislocations necessary for the crystal rotations in the material, hence the term geometrically necessary dislocation density (GND). Statistically stored dislocations (SSD) do not result in crystal curvature and cannot be analysed by EBSD. Figure 1-1 shows schematically the difference between GND and SSD (from Muránský et al. 2019). The dislocations that can be analysed by this technique do not include those parallel to the analysed surface, and EBSD thus underestimates GND. It has, furthermore, been reported (Pantleon 2008) that the true dislocation density, including both GND and SSD, may be a factor of 2 times that analysed by EBSD. The GND value from EBSD can therefore be thought of as a lower limit of both the true GND and the true total dislocation density in the material. Absolute values are complicated to obtain by any method. For better understanding of the absolute value a combination of methods is recommended. TEM studies and XRD analysis yield information on true dislocation density and would be good tools for further analysis.

The dislocation density data emerging from this study will primarily be used in modelling of radiation induced clustering of copper particles in the investigated materials. Since clustering causes unwanted hardening of the material and since clustering is inhibited by high dislocation densities, it is important not to overestimate the densities. This also means that it may be acceptable to obtain the dislocation data from a method like GND that underestimates the density.

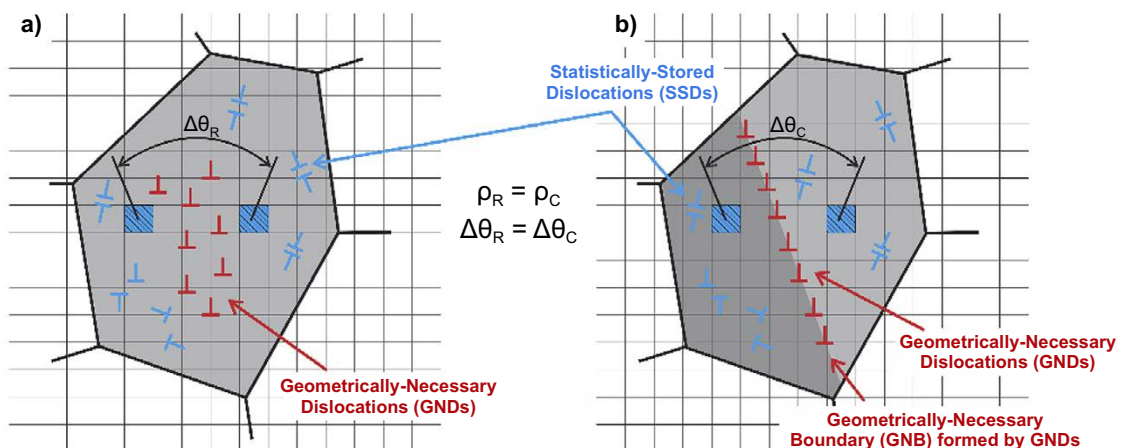


Figure 1-1. Geometrically necessary dislocations (GND) vs statistically stored dislocations (SSD).

2 Investigation

The material in this investigation was P355N, pressure vessel steel grade with good weldability and high resistance to brittle cracking. Composition according to standards is given in Table 2-1. The specimens were taken from large pipes, with diameters of ca 1 000 mm and wall thicknesses of 87 mm. Specimens were cut from two different pipes, denominated ST4 and ST7, and for each sample position specimens were taken in two orientations, radial and circumferential. Specimens were taken at 3 depths; close to the inner surface, at mid position (40 % depth) and close to the outer surface. The number of samples was thus 2 pipes × 2 orientations × 3 positions = 12.

Two data sets were recorded for each sample, one at lower magnification for understanding the overall microstructure (grains and phases etc) and one at higher magnification for dislocation analysis. The EBSD analysis at lower magnification used a step size of 1 µm and the analysis at higher magnification used a 0.1 µm step size. The high magnification analysis areas were chosen to include a high fraction of the ferrite phase since it was the ferrite that was the aim to analyse. The lower magnification analysis covered larger area and was used to guide the position for the high magnification analysis.

The specimens were grinded with 180P-2500P SiC paper and then diamond polished using 6 µm, 3 µm and 1 µm diamond paste. Extreme caution was taken to eliminate all mechanical deformation from the previous grinding/polishing step since any remains of mechanical deformation from surface preparation will affect the EBSD analysis and resulting GND. The final polishing to get rid of all remaining mechanical damage from the last diamond polishing of the surface was done with colloid silica oxide suspension polishing (OP-S) on a rotating disc for 10 minutes. The silica suspension etches the sample chemically and forms a thin brittle oxide on the surface, the silica particles break the oxide and removes it from the surface resulting in a surface free of mechanical deformation.

The electron microscope was a high resolution FEG-SEM, Zeiss GeminiSEM 450. Analyses were done using 20 kV acceleration voltage and 10 nA current. The EDS and EBSD detectors were from Oxford Instruments. The EBSD detector was a Symmetry detector and EDS was Ultim Max. The acquisition and post processing software's were AZtec & AZtec Crystal. The indexing rate was very high, over 98 % in all cases. The data was post processed to close grain boundaries which improves the subsequent analysis of grain sizes.

Table 2-1. Chemical composition (%) of steel P355N (1.0562): EN 10028-3-2009.

According to EN 10216-3:2014: C ≤ 0.2; 0.9 ≤ Mn ≤ 1.7; S ≤ 0.02; N ≤ 0.02; Ti ≤ 0.04;														
C	Si	Mn	Ni	P	S	Cr	Mo	V	N	Nb	Ti	Al	Cu	-
Max 0.18	Max 0.5	1.1–1.7	Max 0.5	Max 0.025	Max 0.015	Max 0.3	Max 0.08	Max 0.1	Max 0.012	Max 0.05	Max 0.03	Max 0.02	Max 0.3	Nb+Ti+V < 0.12

3 Results

Figure 3-1 shows an image of the material ST7 in the axial direction close to the inner surface. The image was made by the back-scattered electron detector (BSED) and shows mainly crystallographic contrast. Pearlite islands with small grains and cementite particles can be seen, and also large ferrite grains. Figure 3-2 shows an EDS map and the distribution of carbon and manganese in the microstructure. Cementite is enriched in carbon (C) and manganese (Mn). The EDS map does not give quantitative numbers on the C and Mn, it is a qualitative way of showing where C and Mn are enriched, bright areas have higher content compared to dark.

The microstructures in the other positions were similarly ferritic/perlitic with large ferrite grains and islands of perlite. The perlite islands showed a sub-structure with smaller ferrite sub-grains and cementite particles embedded in the structure which can be seen in the SEM-BSED image in Figure 3-1. The perlite was not in the form of classic lamellas but mostly rounded cementite particles and also elongated particles in grain boundaries, this can be seen in Figure 3-1 below. The black dots in the image were not analysed in detail, they are etch effects from the silica suspension polishing and the origin is particles.

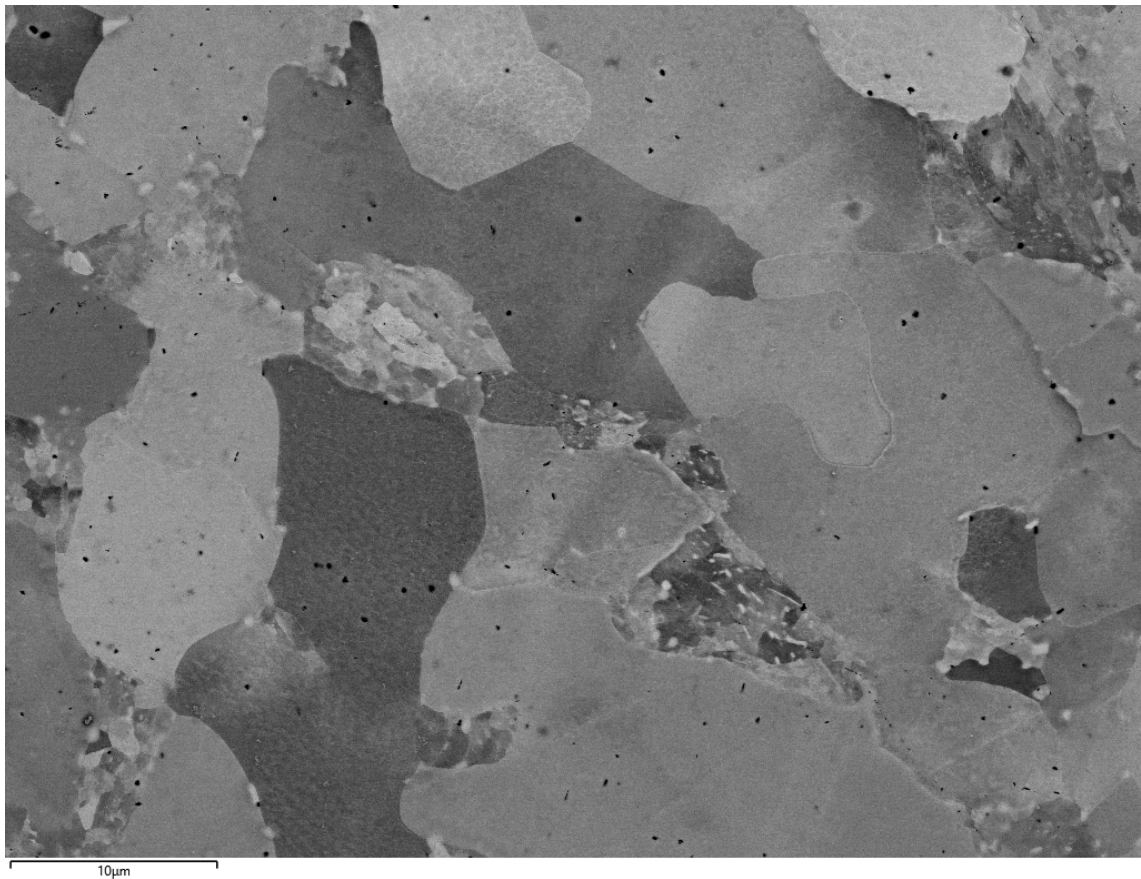


Figure 3-1. BSED image of the microstructure in material ST7 in axial direction showing the large ferrite grains and islands of perlite with small sub-grains and cementite particles.

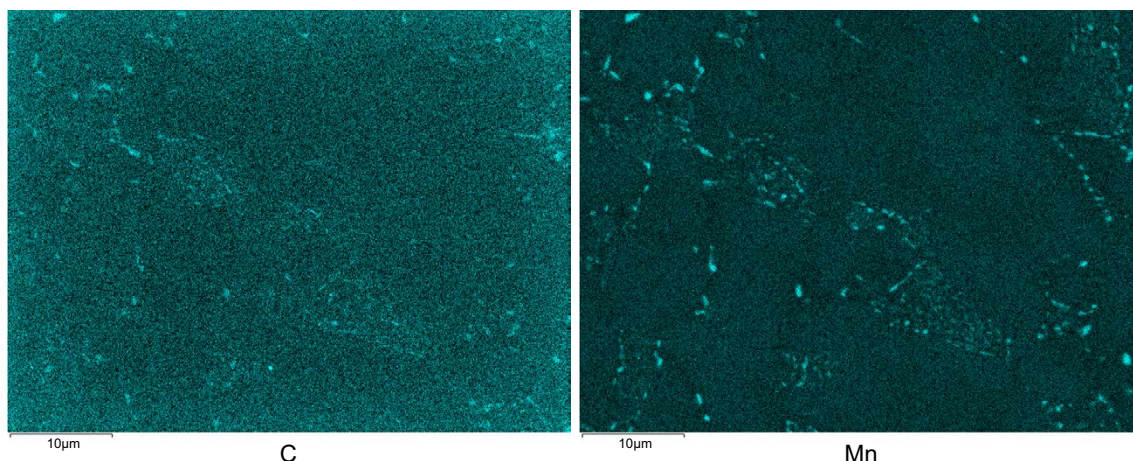


Figure 3-2. EDS mapping analysis showing carbon and manganese distribution of the same area as in Figure 3-1. Cementite contains more carbon and manganese compared to the matrix. Bright areas contains more C or Mn compared to dark areas.

In Figure 3-3 the EBSD analysis for grain size evaluation is shown. Crystallographic directions are illustrated by IPF colouring in the axial direction. The colour key is shown in Figure 3-4. Grain sizes were evaluated for all materials and positions/directions. The grain size distribution and information on number of grains etc for material ST7 in axial direction and close to the inner surface is presented in Figure 3-5. The data for all materials is presented in Table 3-1.

Figure 3-6 shows the EBSD analysis at higher magnification for GND analysis and Figure 3-7 illustrates how the dislocation density is distributed in the material. The GND was higher in the perlite regions where also sub-grain boundaries were frequent. Sub-grains are separated by low angle grain boundaries composed of dislocations. Table 3-2 presents the GND analysis data for all materials. In the GND analysis the Kernell matrix was 3×3 pixels. The threshold for sub-grains was set to 5° . The calculation of GND is affected by several parameters and the threshold for when features are assumed to be dislocations rather than sub-boundaries has a strong effect. The step size during EBSD analysis do also affect the threshold. By lowering the threshold to 2° the apparent GND became about half compared to if the threshold was set to 5° . Figure 3-8 illustrates how the GND distribution looks like using 2° threshold. In this case with the chosen step size ($0.1 \mu\text{m}$) it can be seen (Figure 3-8) that the 2° threshold start to show dislocations and dislocation built sub grains in the ferrite, 2° is therefore a too low value which would exclude a fraction of dislocations from the analysed GND and 5° was therefore chosen as threshold. The corresponding images for all materials and positions/directions are given in the appendix.

In order to obtain a value of the GND that does not overestimate the true value in ferrite, the GND in perlite need to be removed and not included in the averaging of the GND. The perlite fraction was lower than 10 % and by excluding the highest 10 % of the values from the data set of each sample a measure that does not overestimate the GND in ferrite can be evaluated. The average GND in the remaining 90 % (the ferrite) is presented in Table 3-3 for all samples and can be understood as a lower bound GND, a measure that does not overestimate the GND in ferrite.

Table 3-1. Grain sizes as equivalent circle diameters. Arithmetic mean and area weighted mean.

Ave grain size Arit/Weight	ST7 AX (μm)	ST7 CIRC (μm)	ST4 AX (μm)	ST4 CIRC (μm)
Inner surf	8.3/16.2	8.8/17.0	8.4/18.5	8.4/18.0
Mid	8.4/18.0	9.2/19.6	8.8/18.6	8.1/18.0
Outer surf	8.6/21.5	8.8/18.5	9.2/18.3	7.3/15.4

Table 3-2. Fraction of the analysed area with lowest dislocation density and maximum GND in the analysis.

GND ($\times 10^{14}$) % in Bin 1/Max	ST7 AX (%/GND)	ST7 CIRC (%/GND)	ST4 AX (%/GND)	ST4 CIRC (%/GND)
Inner surf	96.2/63.2	95.3/64.3	95.4/64.4	93.6/58.9
Mid	88.5/64.4	96.0/61.7	96.3/64.0	95.2/61.3
Outer surf	94.3/64.2	95.8/63.4	93.7/63.7	96.4/62.7

Table 3-3. Average GND in ferrite.

GND ($\times 10^{14}$) Average in ferrite	ST7 AX	ST7 CIRC	ST4 AX	ST4 CIRC
Inner surf	1.8	2.8	3.8	2.8
Mid	4.2	2.2	2.9	3.4
Outer surf	3.0	2.5	3.1	3.2

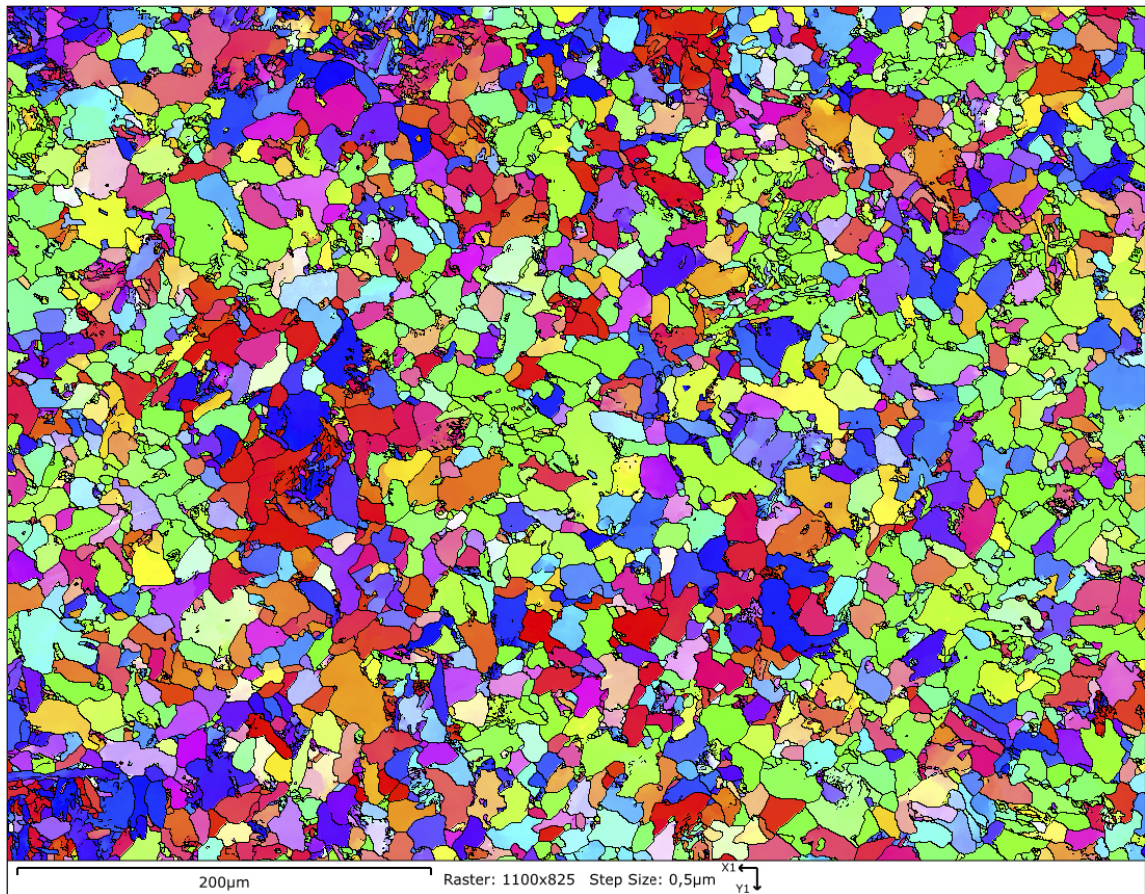


Figure 3-3. EBSD map at low magnification for grain size analysis. Colours according to crystal orientations by IPF colour key. Grain boundaries $\geq 2^\circ$ present as black lines.

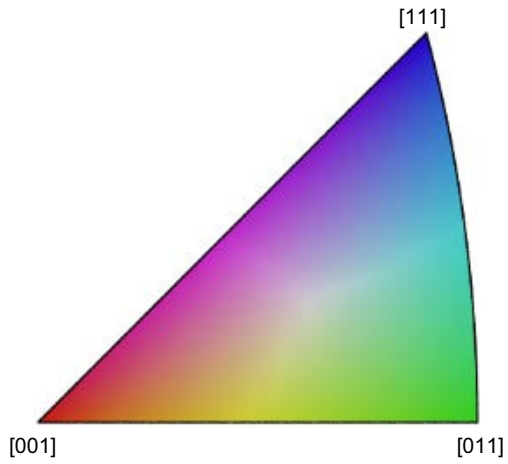


Figure 3-4. Inverse pole figure (IPF) colour key.

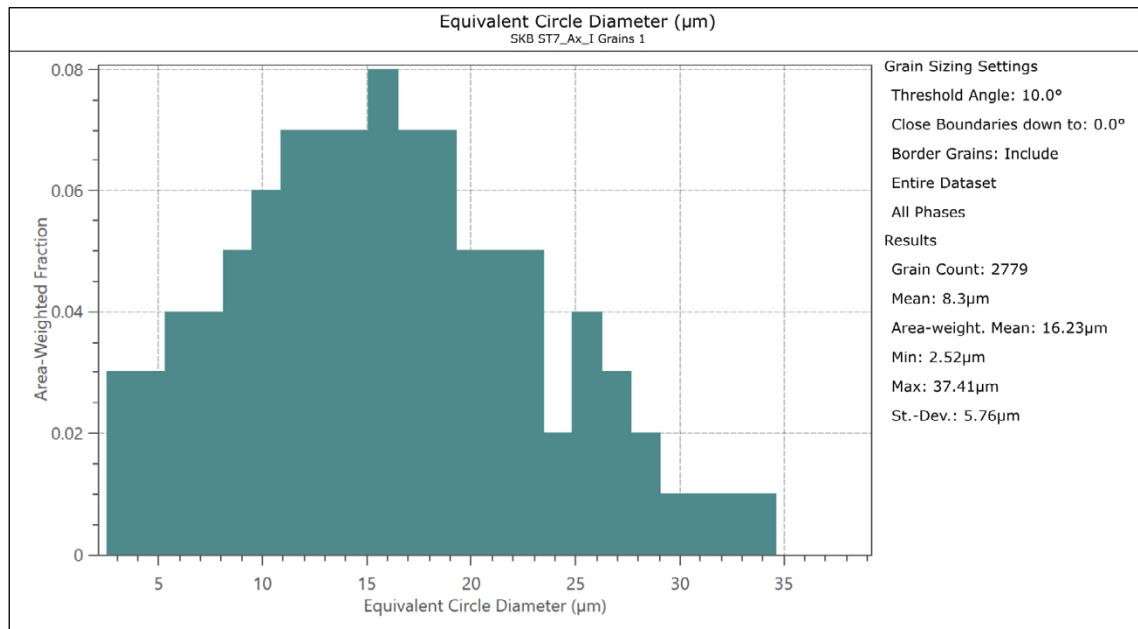


Figure 3-5. Grain size distribution for material ST7 in axial direction close to the inner surface.

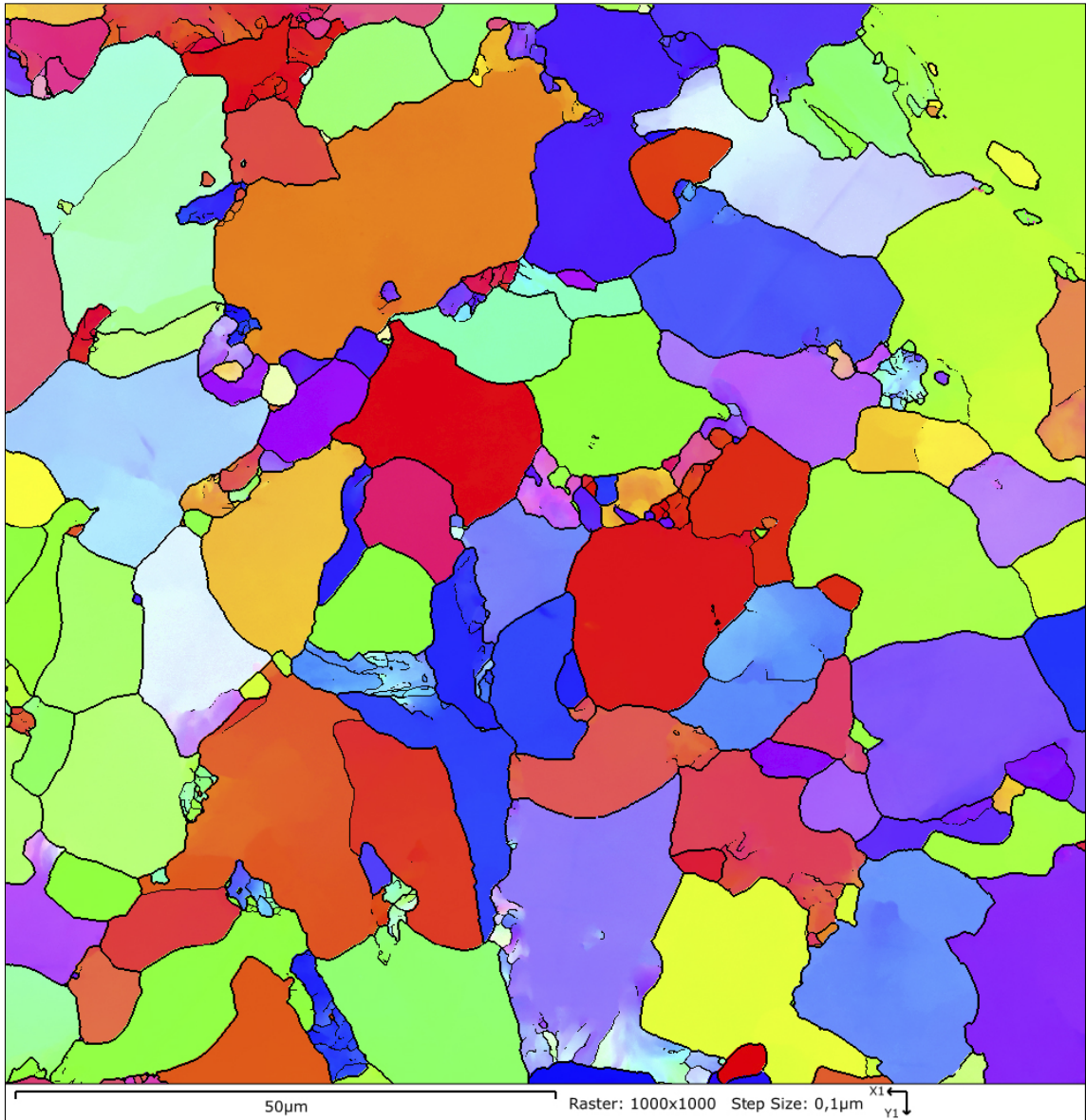


Figure 3-6. EBSD map at high magnification for dislocation density (GND) analysis. Colours according to crystal orientations by IPF colour key. Grain boundaries $\geq 2^\circ$ thin black lines and grain boundaries $\geq 10^\circ$ thick black lines.

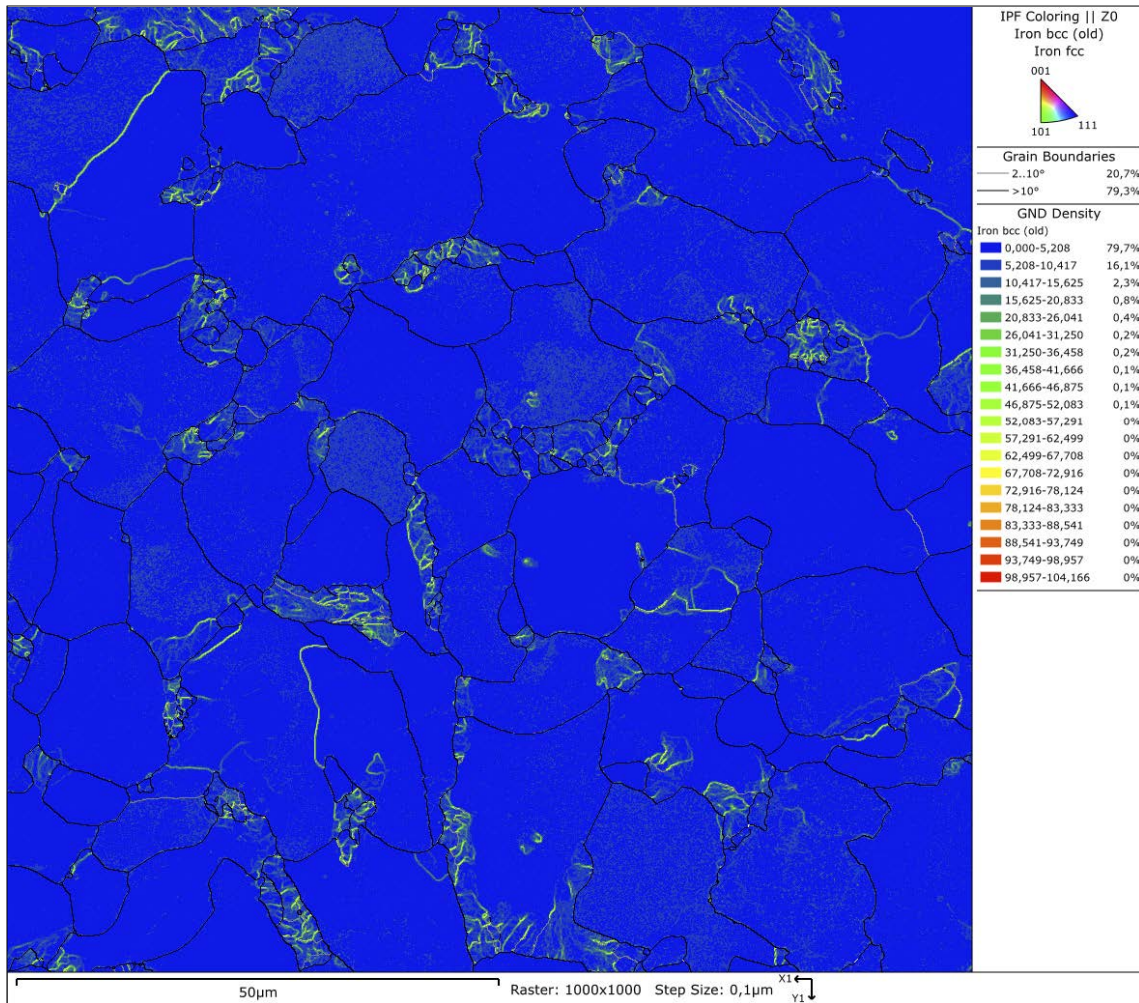


Figure 3-7. EBSD map at high magnification for dislocation density (GND) analysis. The areas with high GND corresponds to the perlitic areas in the material. GND analysis with Kernell size 3×3 and 5° threshold for sub-grains.

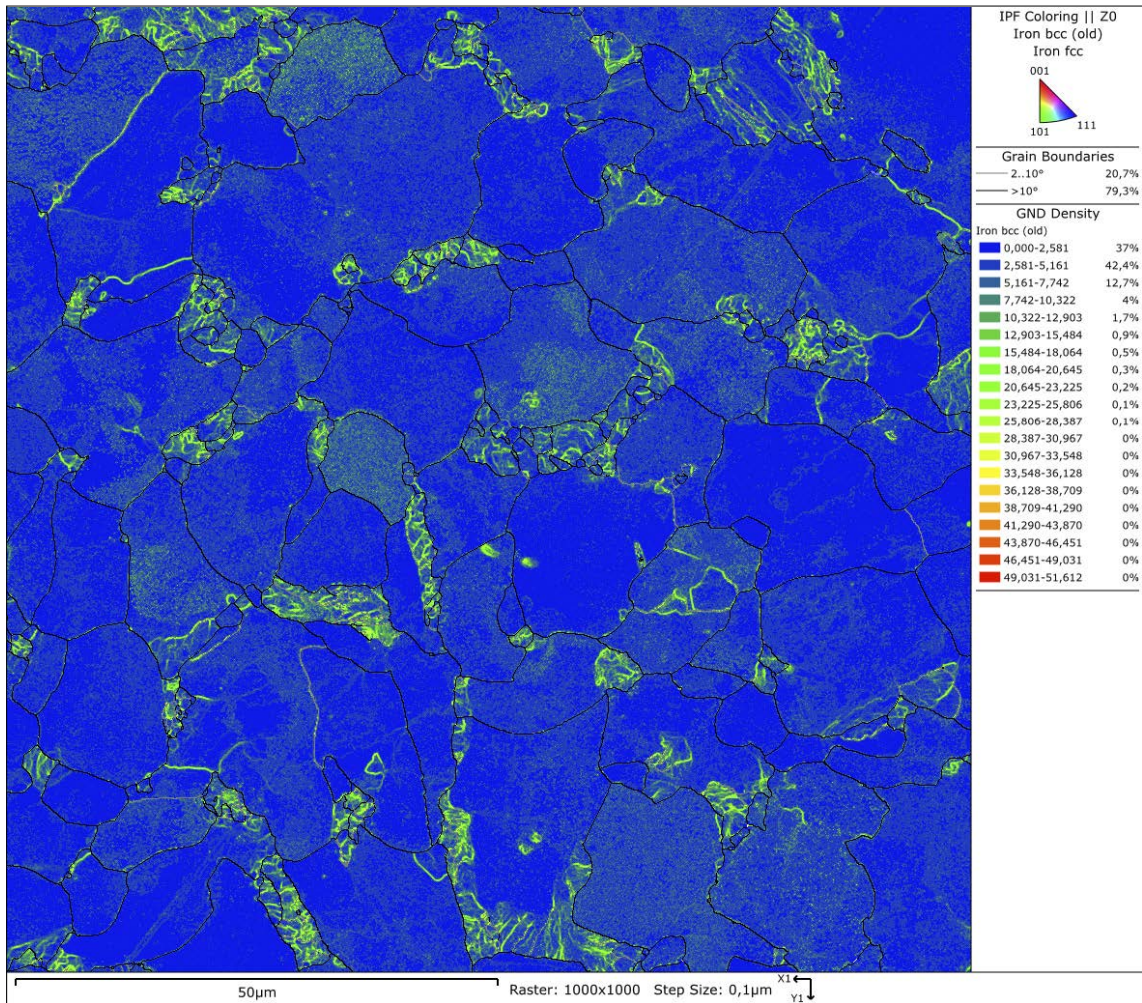


Figure 3-8. Same plot as in Figure 3-7, but the GND analysis was performed with 2° threshold for sub-grains.

4 Conclusions

The average GND in ferrite was $2-4 \times 10^{14} \text{ m}^{-2}$ which was considerably lower compared to the perlite where the GND was around $50 \times 10^{14} \text{ m}^{-2}$. There was no consistent difference in GND between the different tubes and positions/directions. The areas with low GND ($0-9.5 \times 10^{14} \text{ m}^{-2}$) corresponded well to the ferritic areas and made up between 87 % and 96 % of the total area. The variation between the samples was mostly due to variations in the fraction of perlite in the analysed area. The maximum GND varied from 61.8×10^{14} to $64.4 \times 10^{14} \text{ m}^{-2}$ between the samples.

An important result from this study was also that the GND in perlite areas was considerably higher compared to the ferrite areas. Additionally, the perlite contained dislocation sub-boundaries which was not present in the ferrite. This understanding will be important if dislocation density analysis with more local techniques, i.e. TEM were to be carried out.

5 Discussion

There are many papers written on dislocation analysis using EBSD, but to this author's knowledge there is no published experimental work where quantitative analysis of dislocation densities from different methods are compared. Most papers include theoretical treatments on dislocations and how EBSD can be used to analyse dislocations. The term weighted burgers vector analysis is used due to the fact that dislocations parallel to the analysed surface or with a low angle to the surface cannot be analysed or are not analysed to the same degree as dislocations that are at a high angle to the analysed surface. According to reference 3, the true dislocation density can be estimated to be a factor of 2 higher than that analysed by EBSD. This was confirmed by private discussions with P Trimby, Oxford instruments. Trimby has compared TEM analysis with EBSD and found that EBSD gave GND values about half of what TEM analysis gave.

6 Potential further work

TEM analysis could be used to quantitatively confirm the findings in the work where GND was analysed using EBSD.

Further work with improved data quality analysis using EBSD would give new insights into the distribution of GND in the ferrite. Pattern matching can be used to improve the angular resolution of the EBSD analysis from about 0.15° in the present work to below 0.05° using pattern matching.

References

SKB's (Svensk Kärnbränslehantering AB) publications can be found at www.skb.com/publications.

Konijnenberg P J, Zaefferer S, Raabe D, 2015. Assessment of geometrically necessary dislocation levels derived by 3D EBSD. *Acta Materialia* 99, 402–414.

Electron Backscatter Diffraction, 2024a. Basics of Automated Indexing. Oxford: Oxford Instruments plc.

Electron Backscatter Diffraction, 2024b. High Precision Electron Backscatter Diffraction (EBSD). Oxford: Oxford Instruments plc.

Electron Backscatter Diffraction, 2024c. Dislocation Analysis. Oxford: Oxford Instruments plc.

Muránsky O, Balogh L, Tran M, Hamelin C J, Park J S, Daymond M R, 2019. On the measurement of dislocations and dislocation substructures using EBSD and HRSD techniques. *Acta Materialia* 75, 297–313.

Pantleon W, 2008. Resolving the geometrically necessary dislocation content by conventional electron backscattering diffraction. *Scripta Materialia*. 58, 994–997.

Wheeler J, Mariani E, Piazzolo S, Prior D J, Trimby P, Drury M R, 2009. The weighted Burgers vector: a new quantity for constraining dislocation densities and types using electron backscatter diffraction on 2D sections through crystalline materials. *Journal of Microscopy* 233, 482–494.

Images for all materials and positions/directions

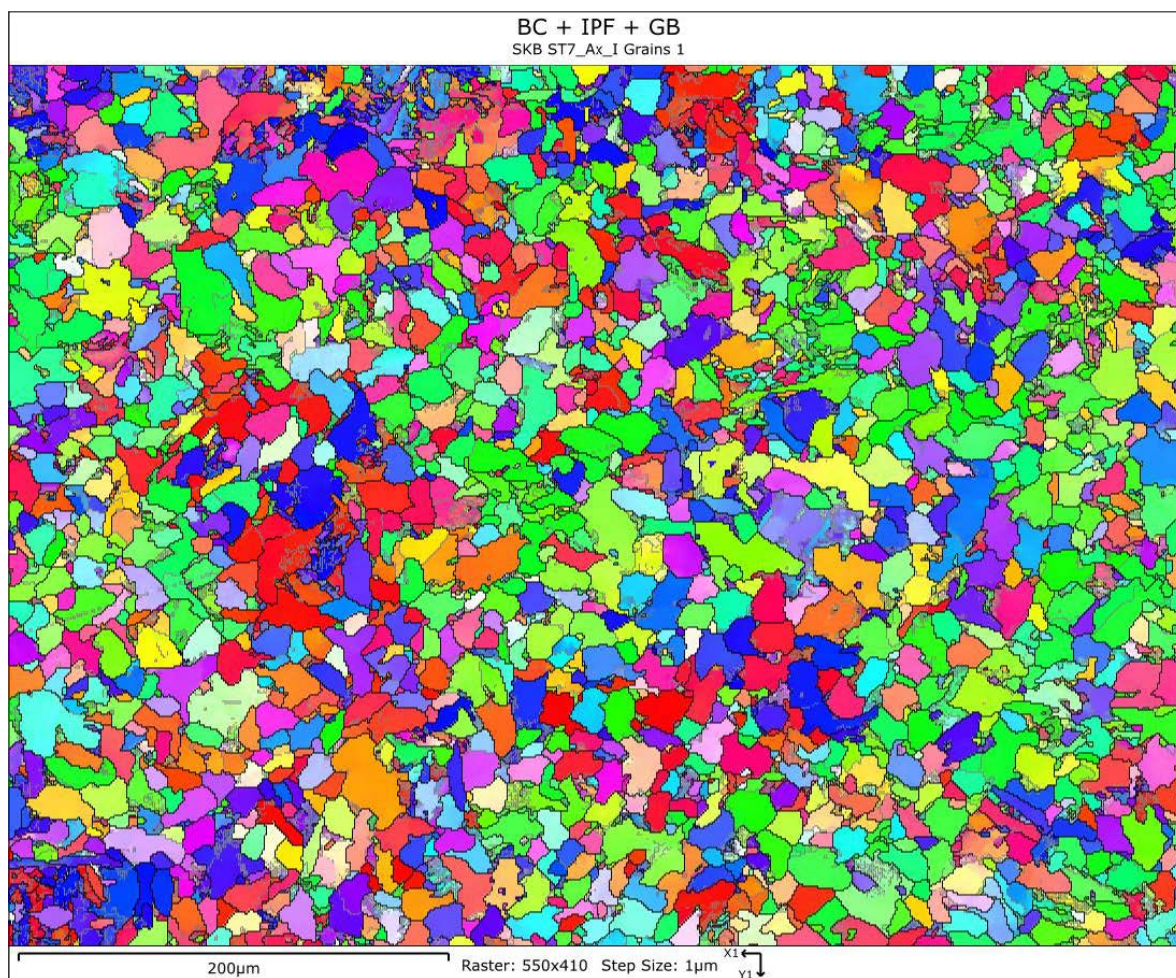


Figure A-1. Specimen ST7 in axial direction. Close to inner surface. Lower magnification EBSD analysis showing the grain structure.

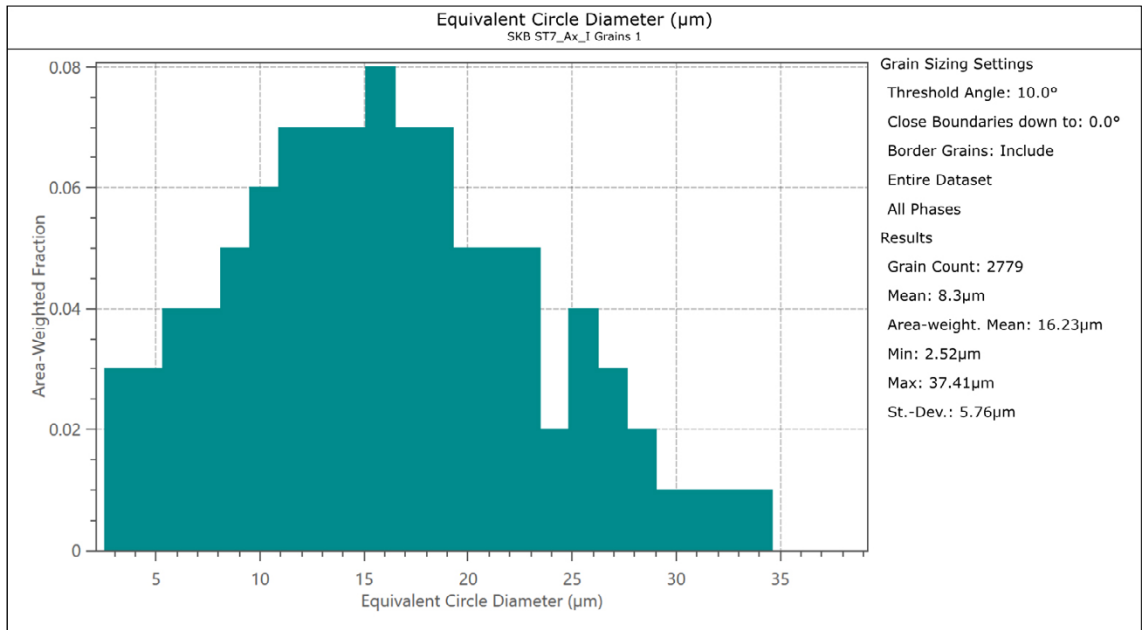


Figure A-2. ST7 in axial direction, inner surface.

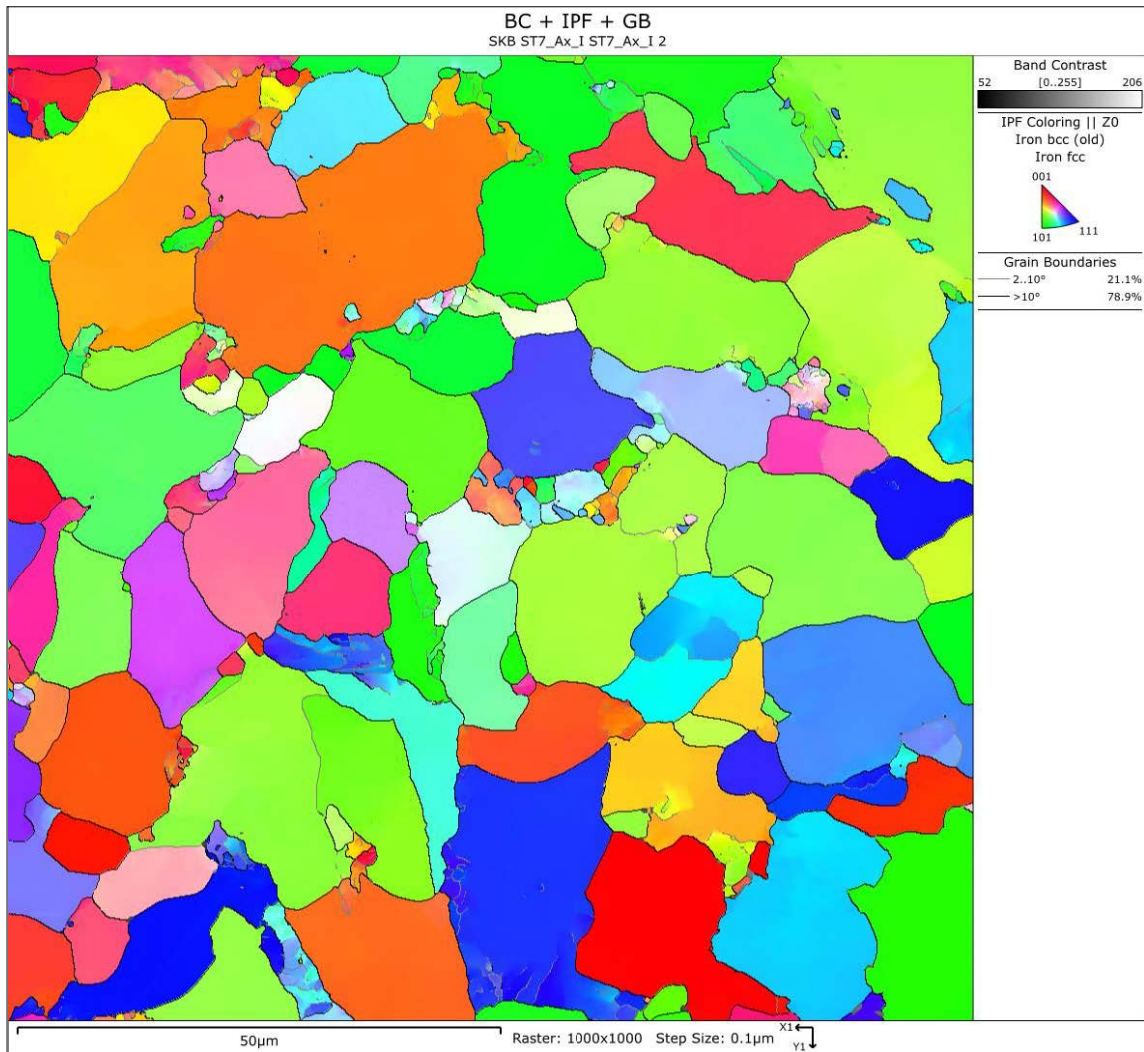


Figure A-3. Specimen ST7 in axial direction. Close to inner surface. Higher magnification EBSD analysis for dislocation analysis.

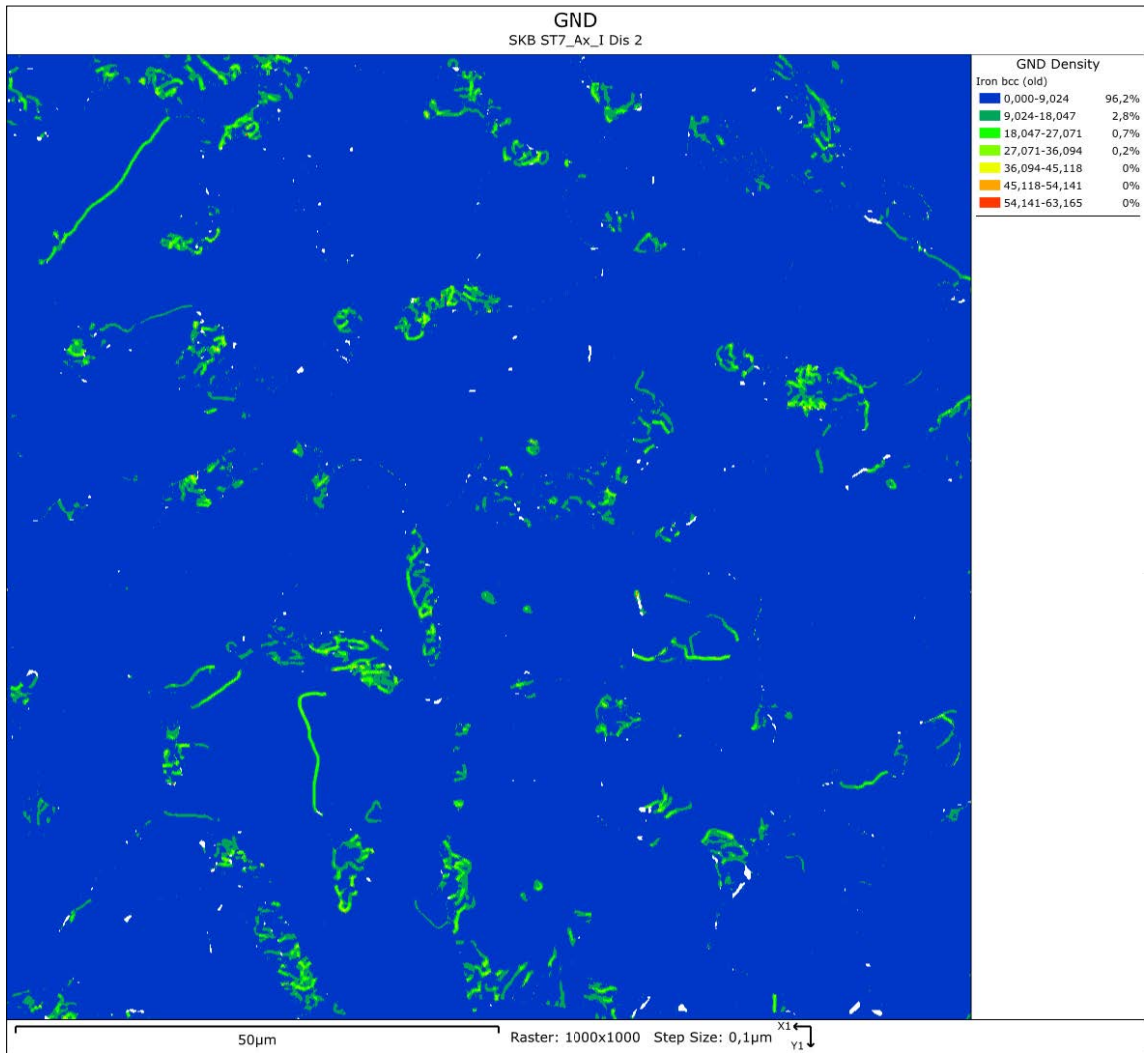


Figure A-4. ST7 in axial direction, inner surface.

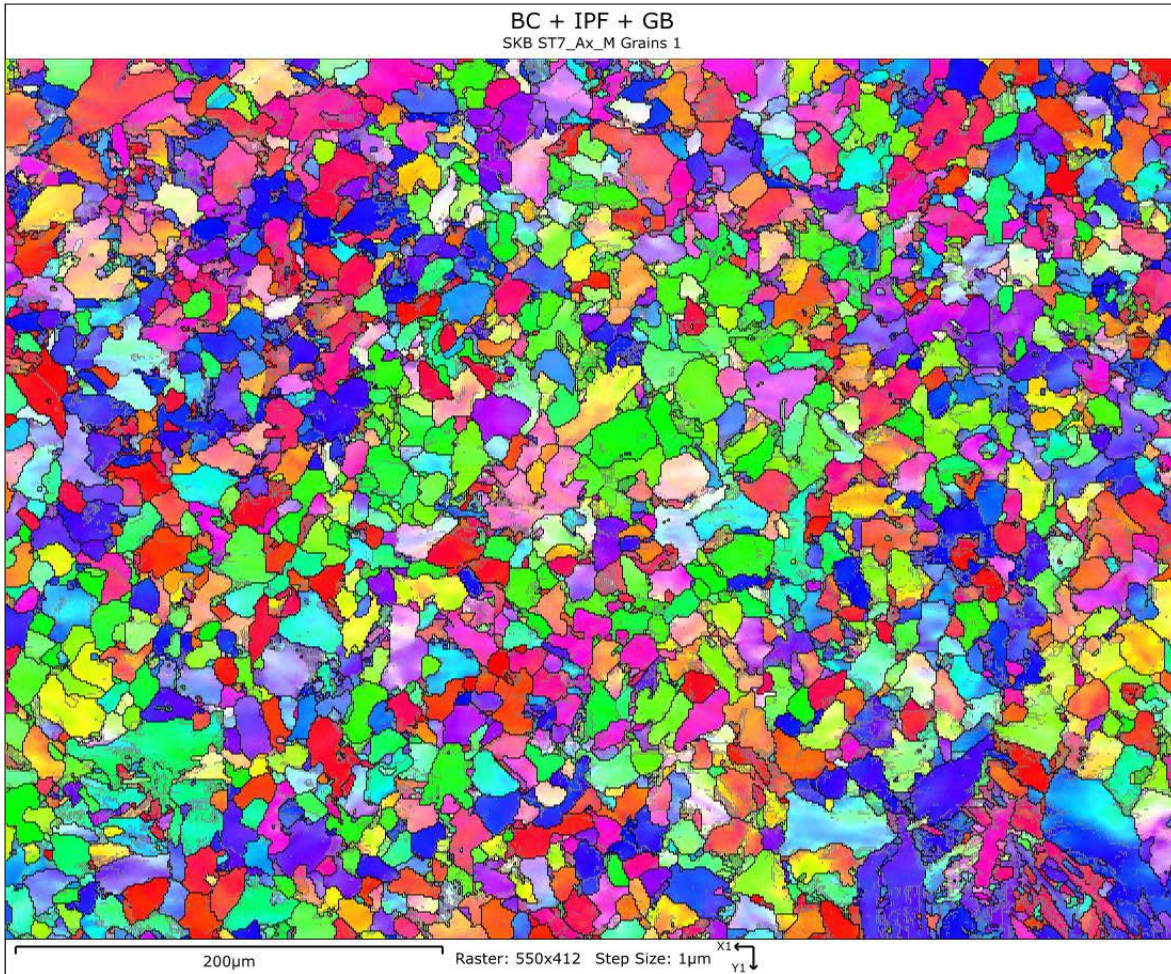


Figure A-5. Specimen ST7 in axial direction. Mid position. Lower magnification EBSD analysis showing the grain structure.

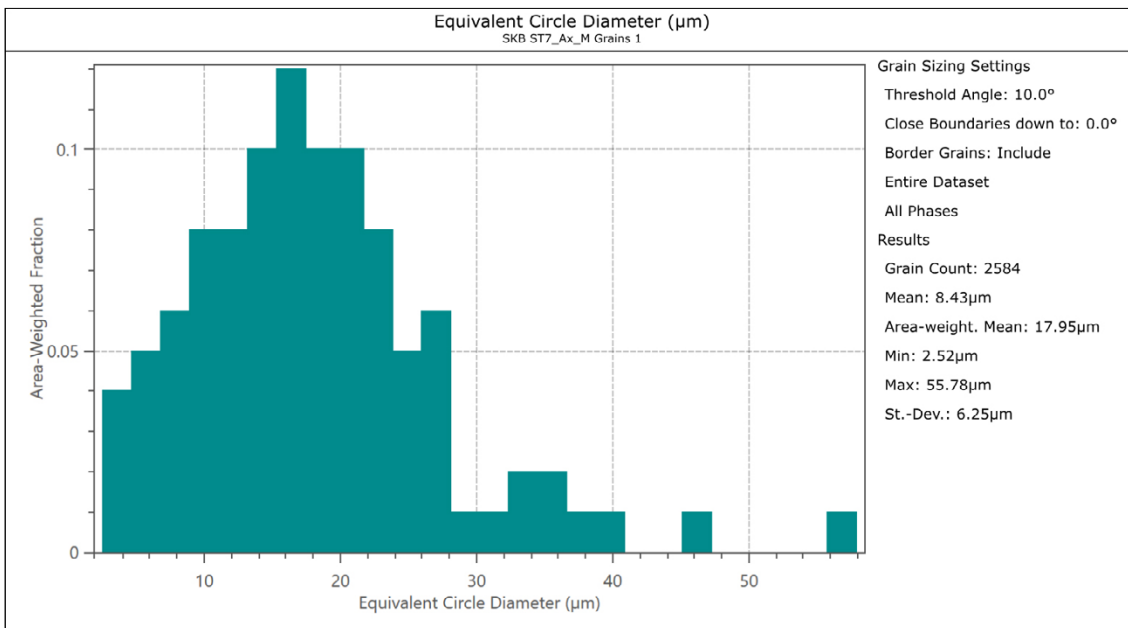


Figure A-6. ST7 in axial direction, mid position.

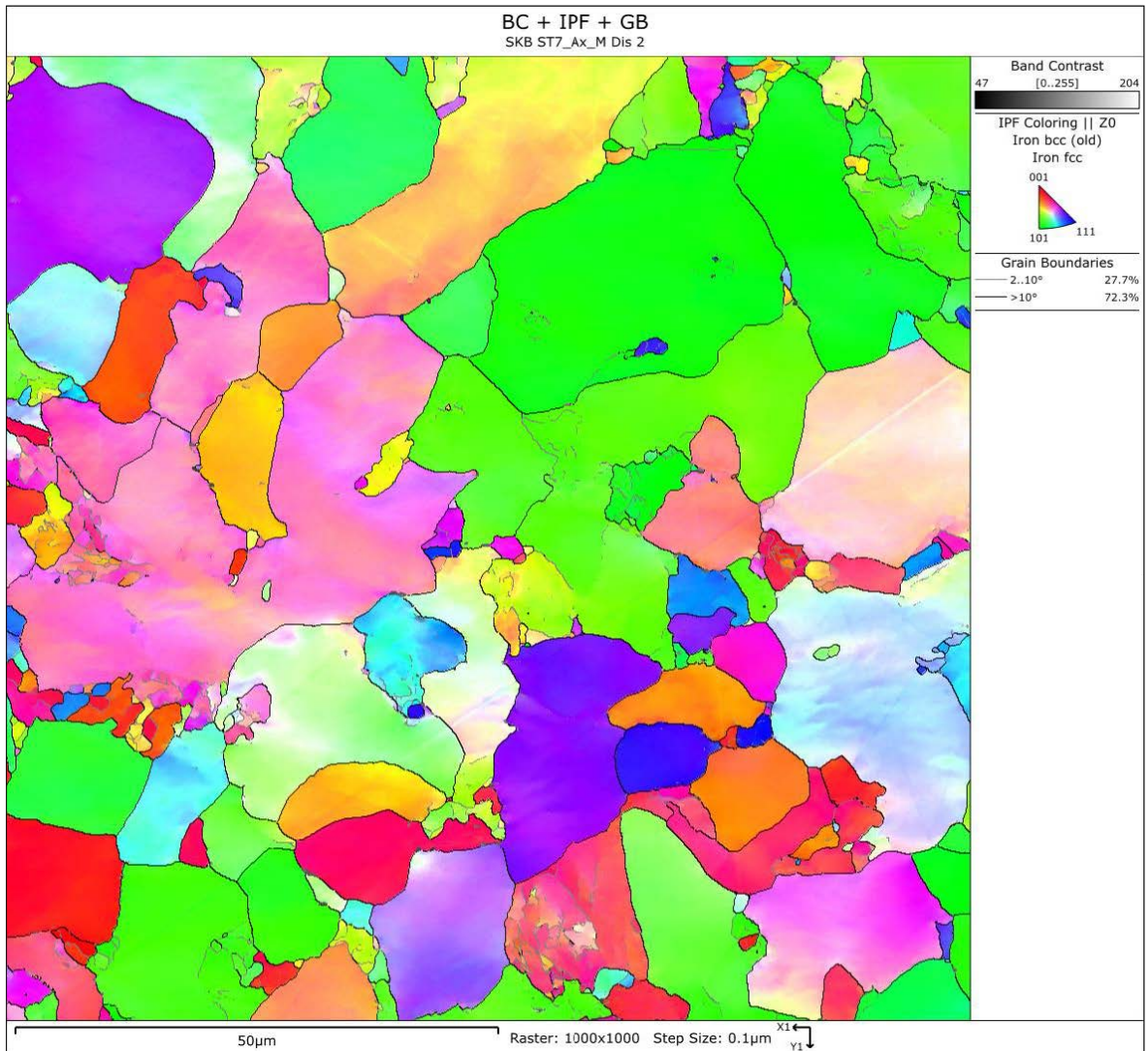


Figure A-7. Specimen ST7 in axial direction. Mid position. Higher magnification EBSD analysis for dislocation analysis.

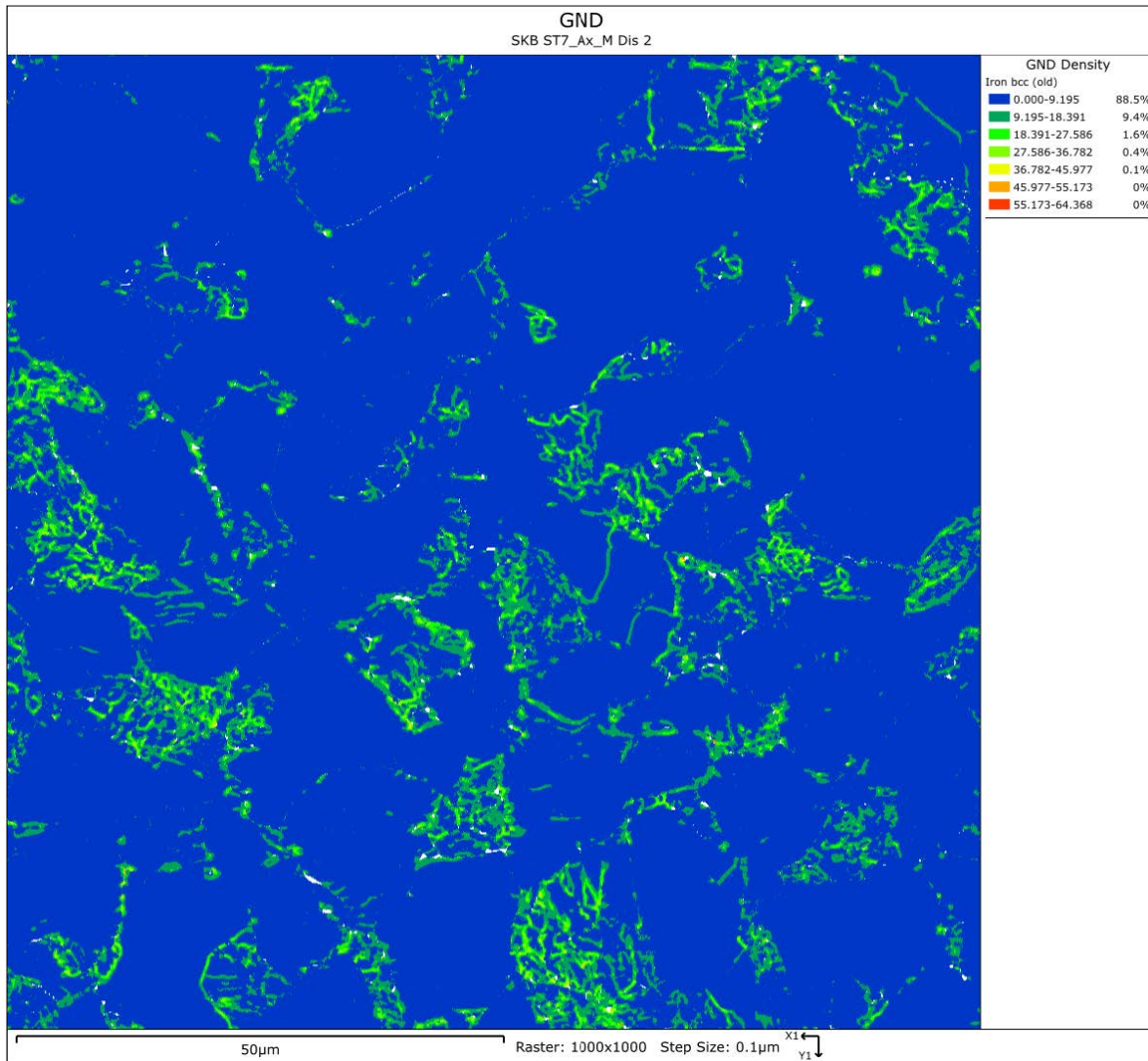


Figure A-8. ST7 in axial direction, Mid position.

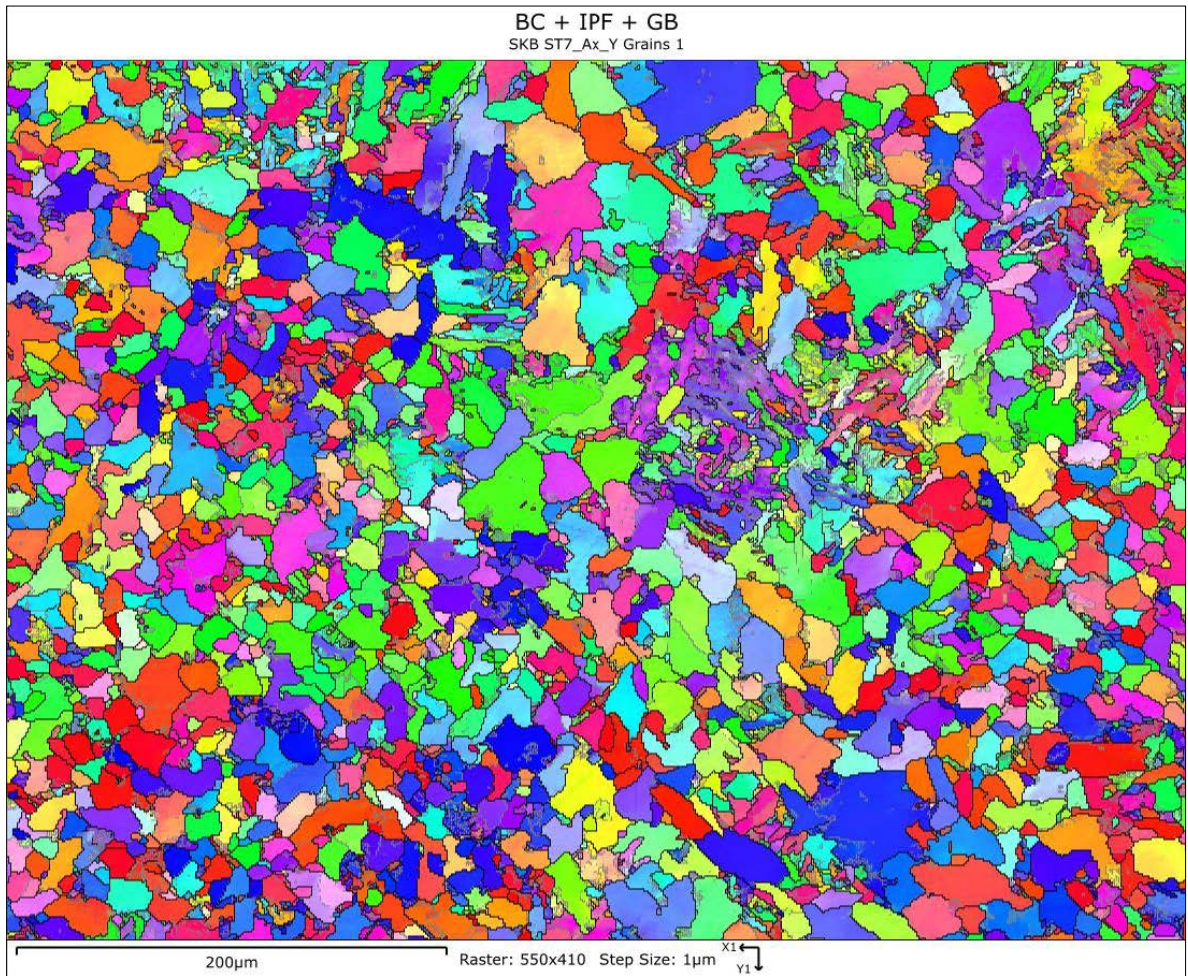


Figure A-9. Specimen ST7 in axial direction. Close to outer surface. Lower magnification EBSD analysis showing the grain structure.

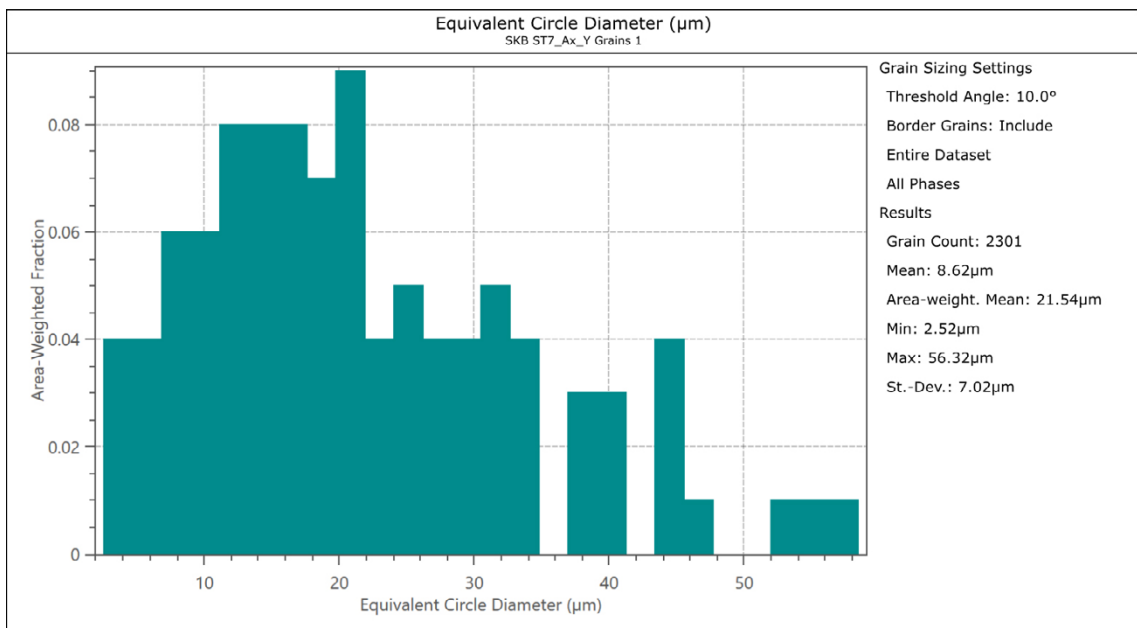


Figure A-10. ST7 in axial direction, outer surface.

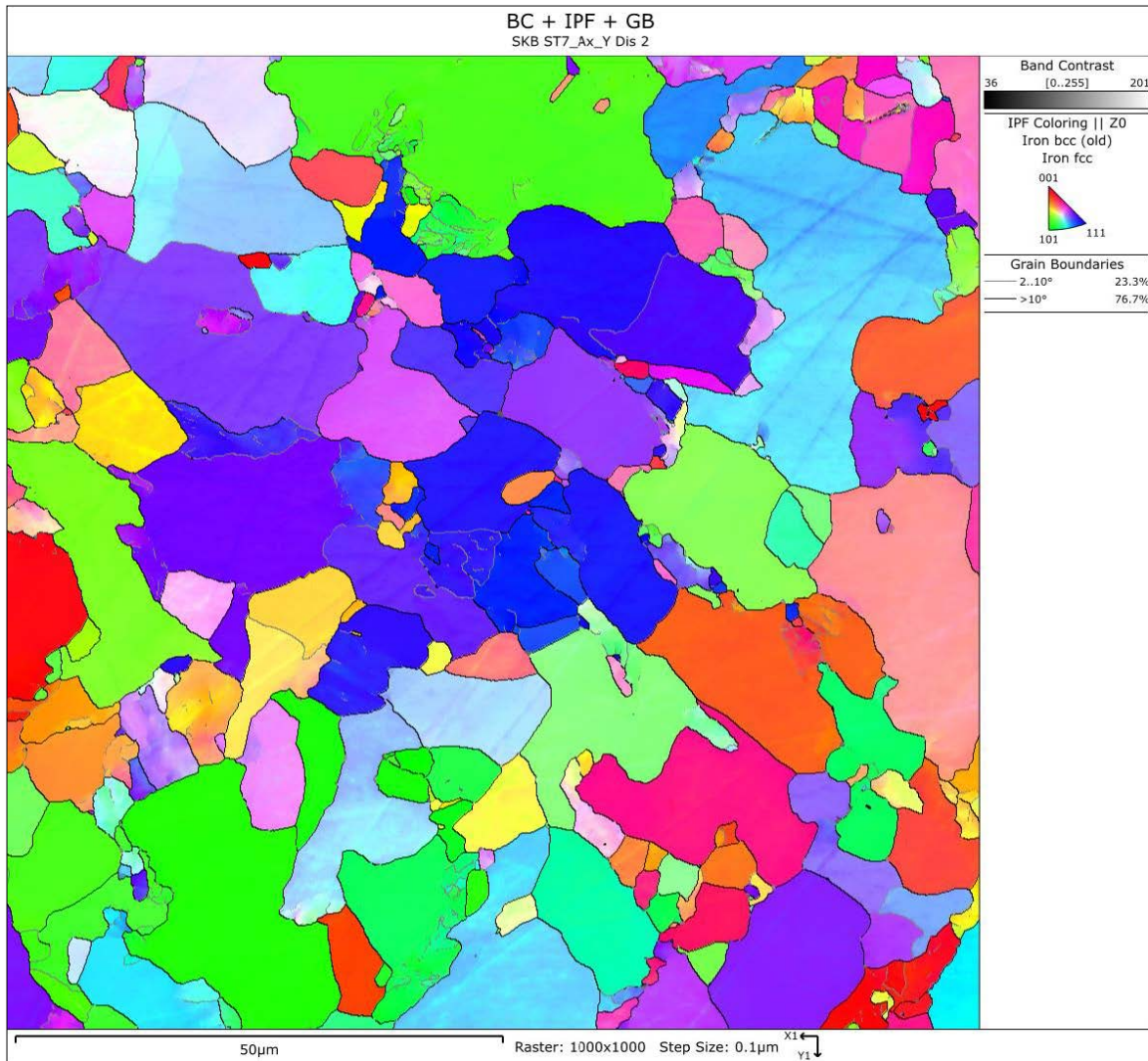


Figure A-11. Specimen ST7 in axial direction. Close to outer surface. Higher magnification EBSD analysis for dislocation analysis.

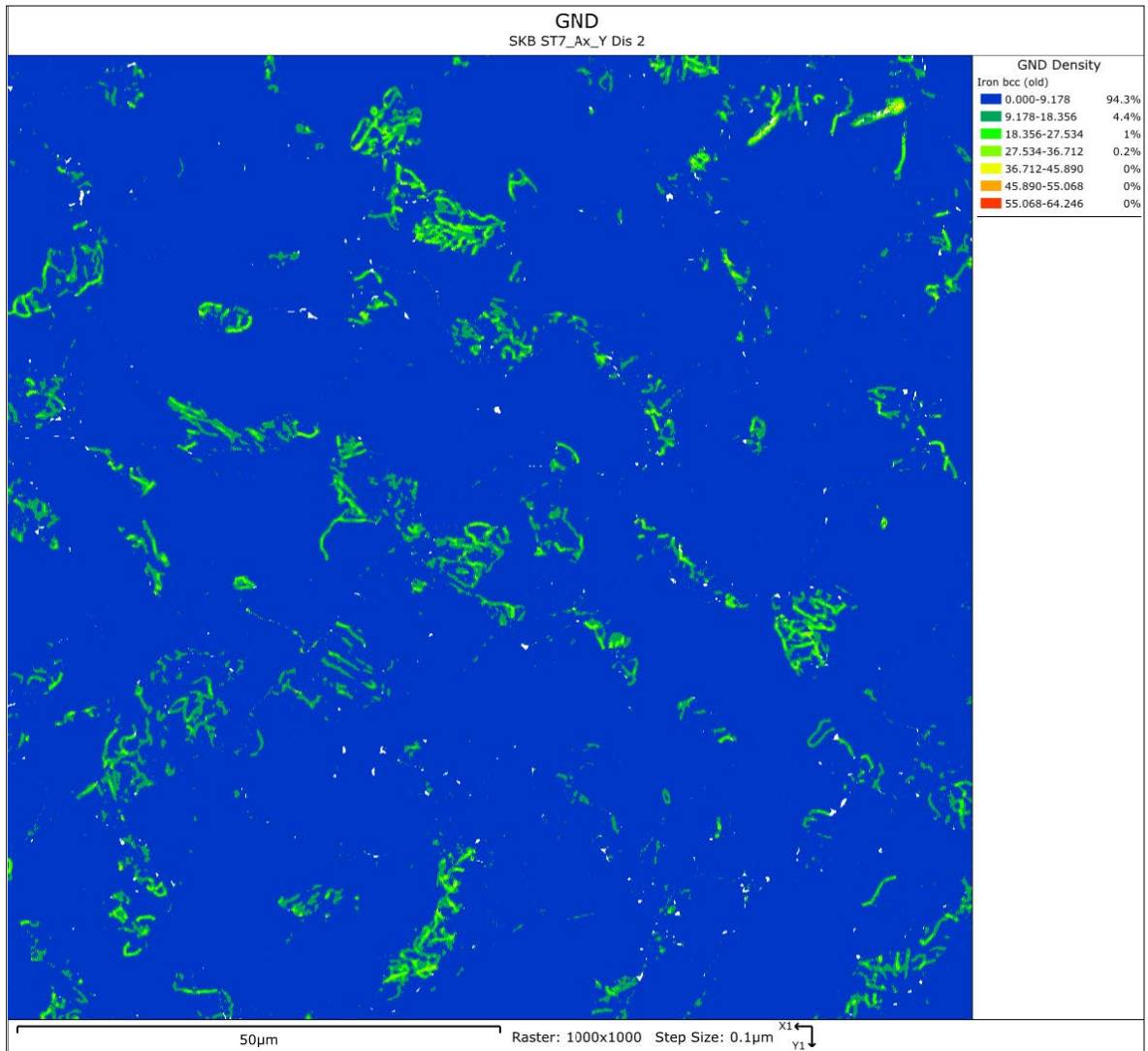


Figure A-12. ST7 in axial direction. Outer surface.

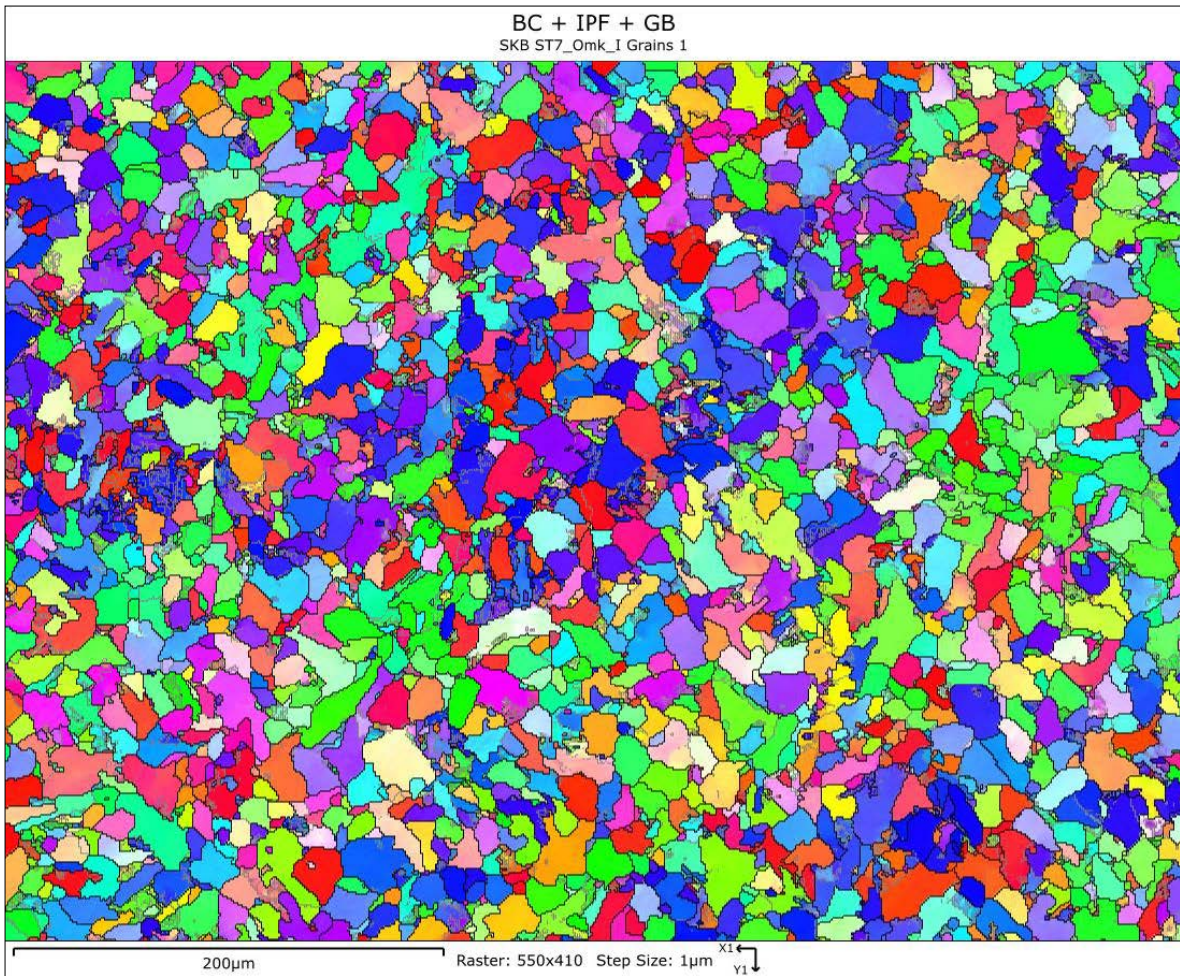


Figure A-13. Specimen ST7 in circumferential direction. Close to inner surface. Lower magnification EBSD analysis showing the grain structure.

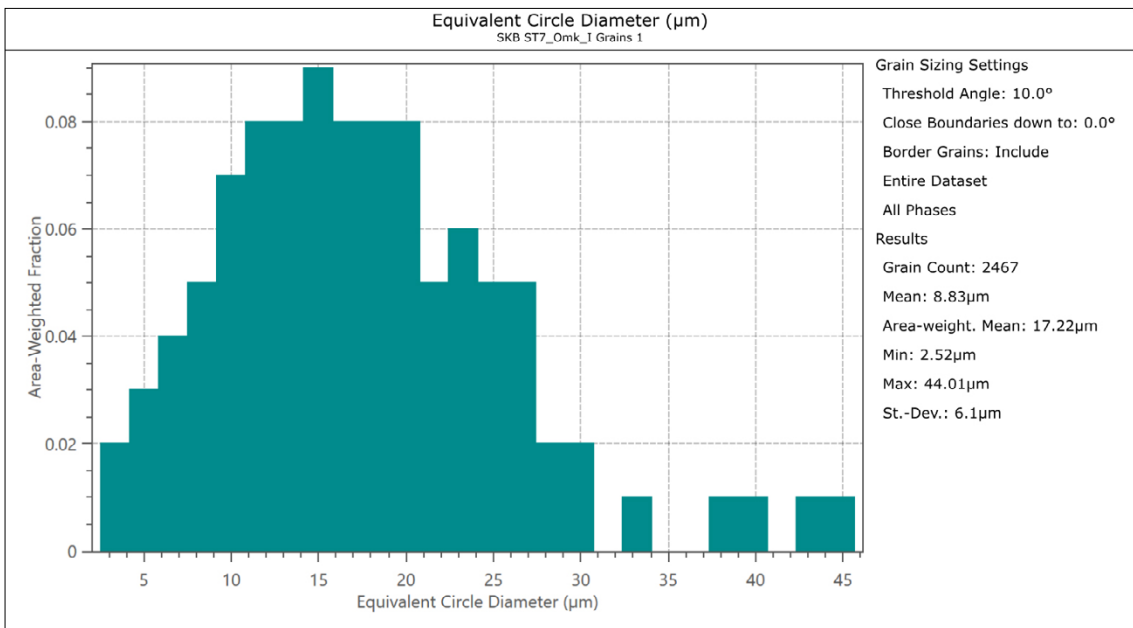


Figure A-14. ST7 circumferential direction, inner surface.

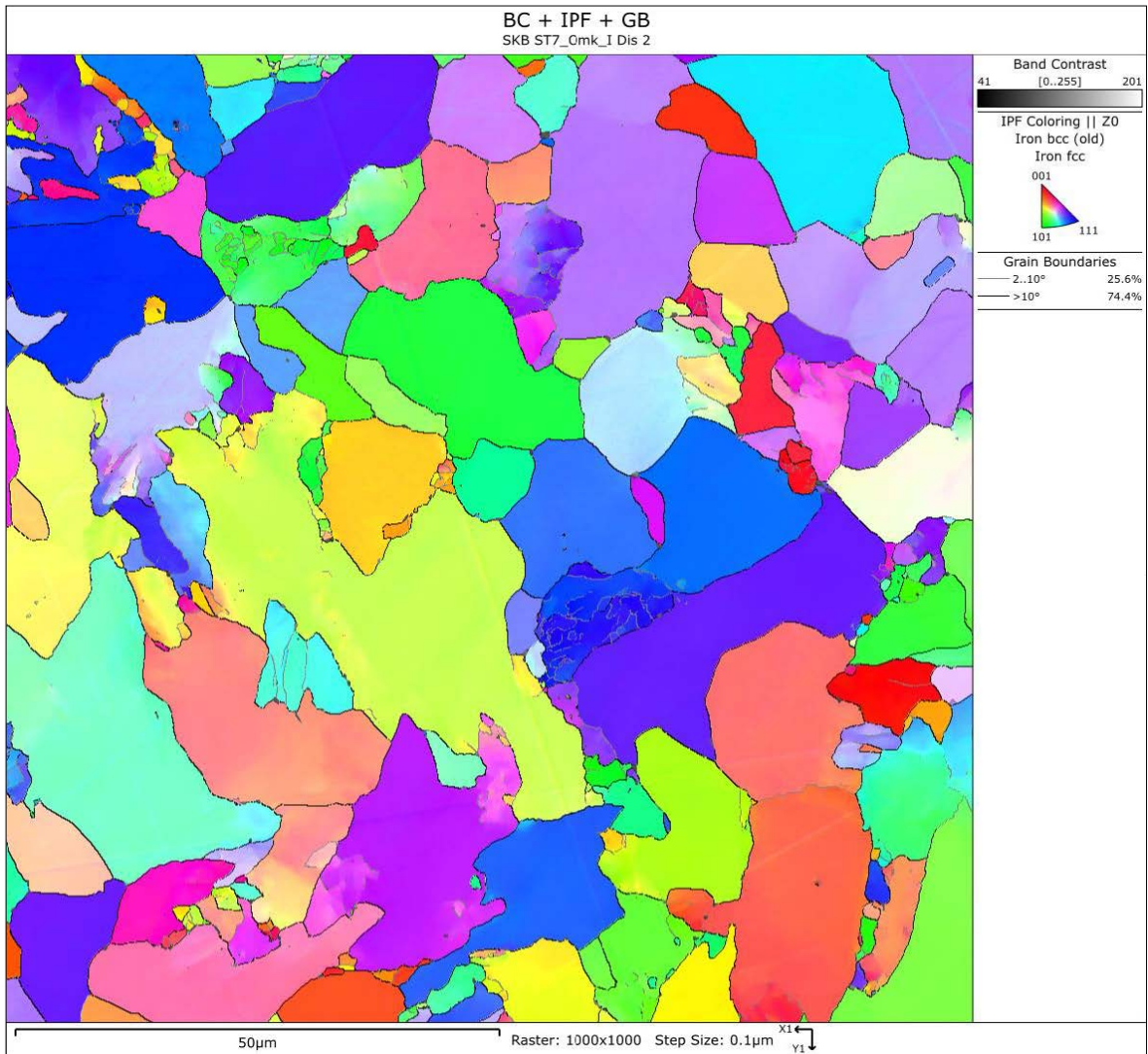


Figure A-15. Specimen ST7 in circumferential direction. Close to inner surface. Higher magnification EBSD analysis for dislocation analysis.

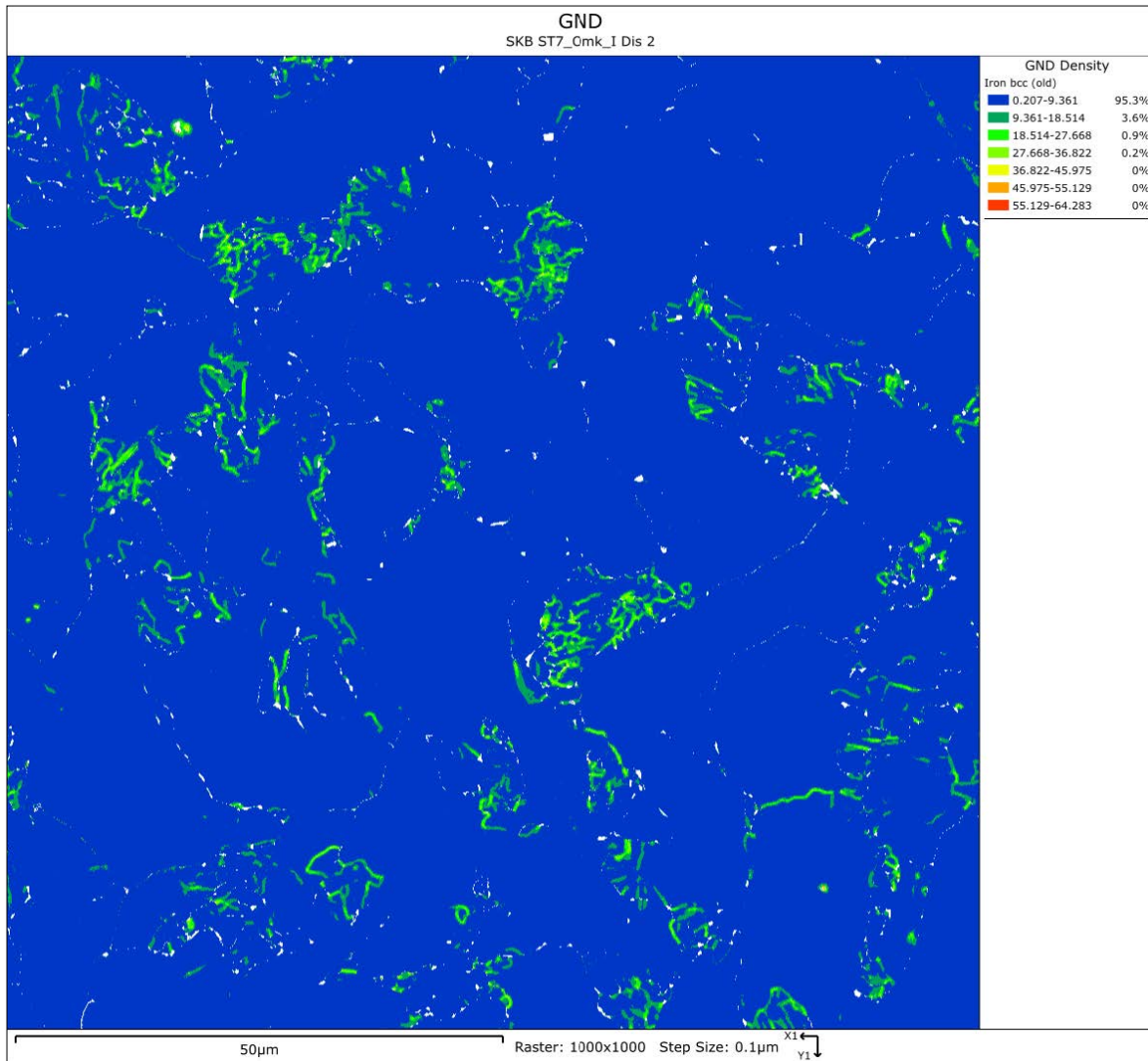


Figure A-16. ST7 circumferential direction, inner surface.

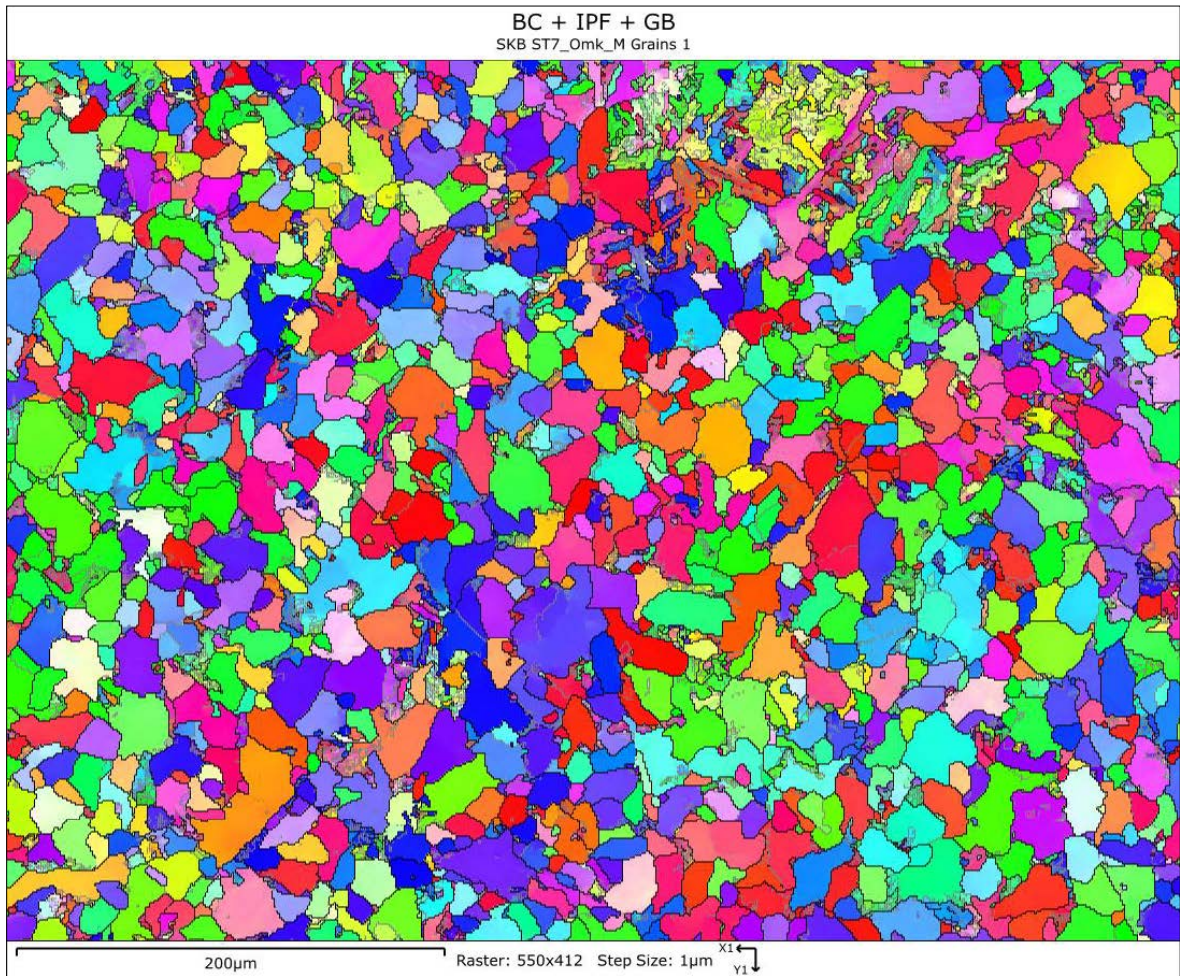


Figure A-17. Specimen ST7 in circumferential direction. Mid position. Lower magnification EBSD analysis showing the grain structure.

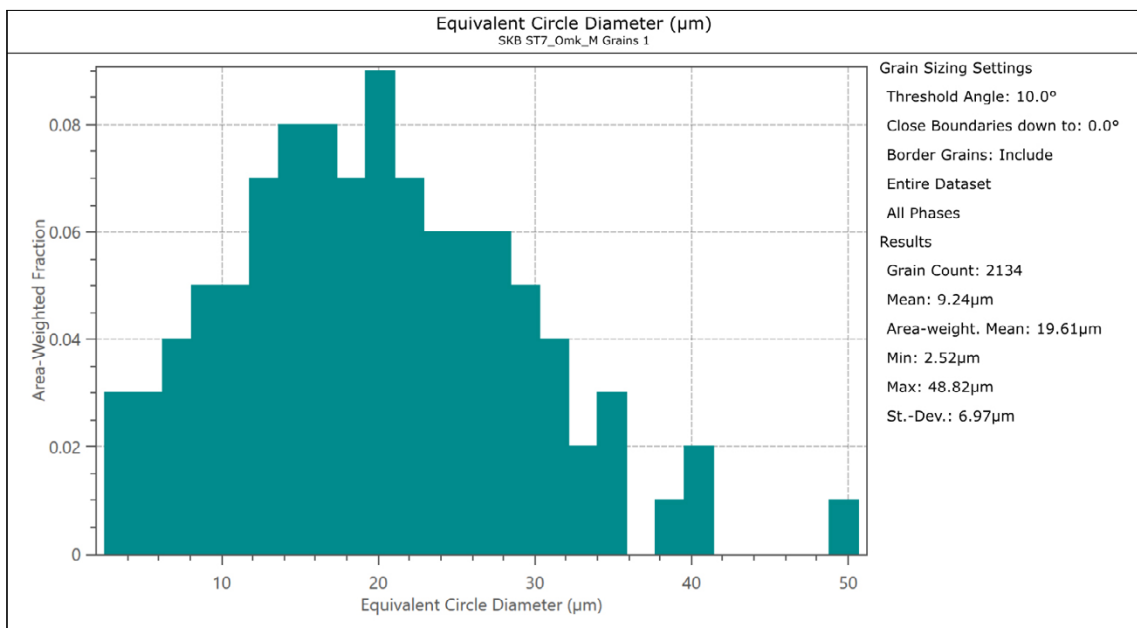


Figure A-18. ST7 circumferential direction, mid position.

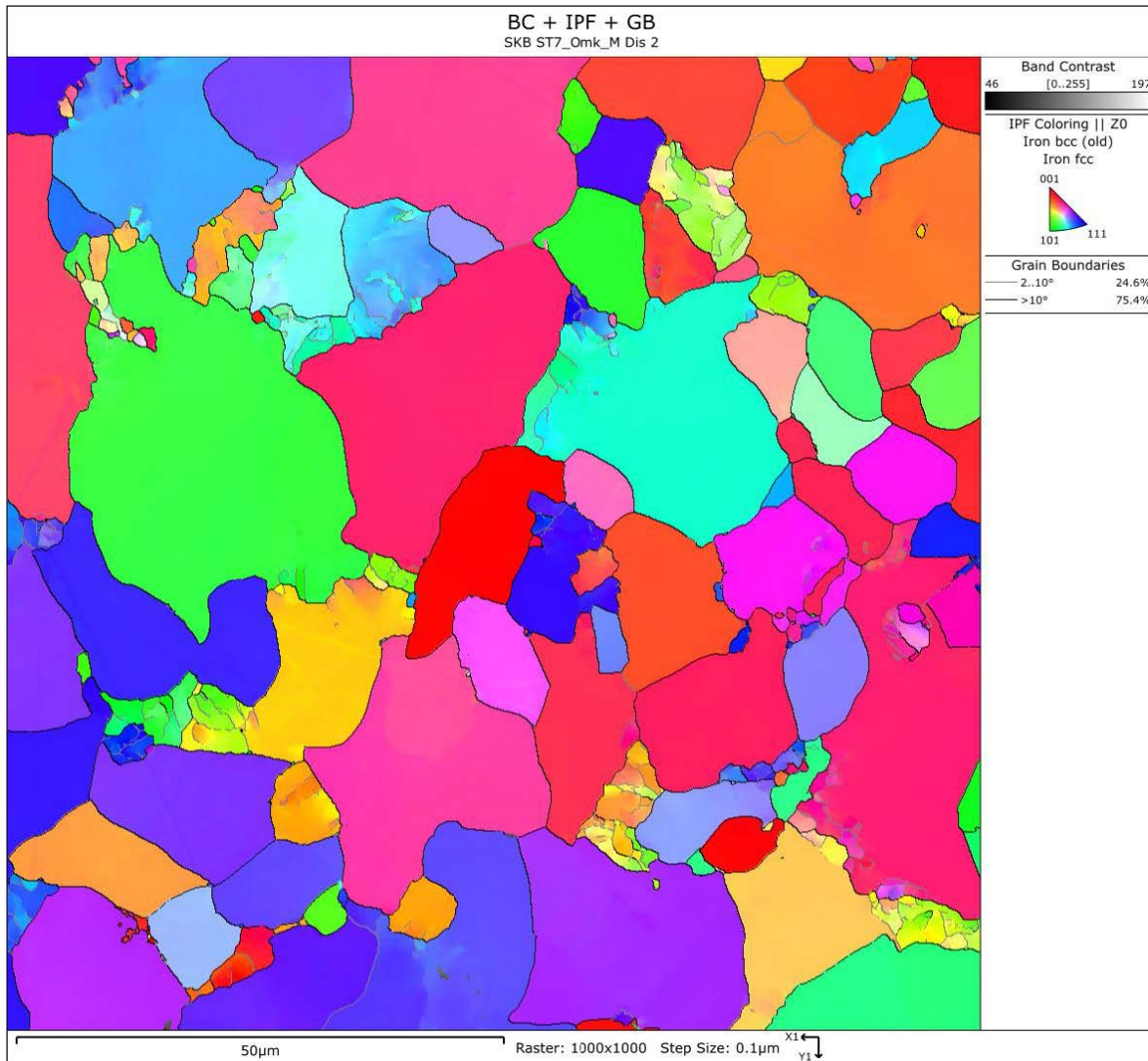


Figure A-19. Specimen ST7 in circumferential direction. Mid position. Higher magnification EBSD analysis for dislocation analysis.

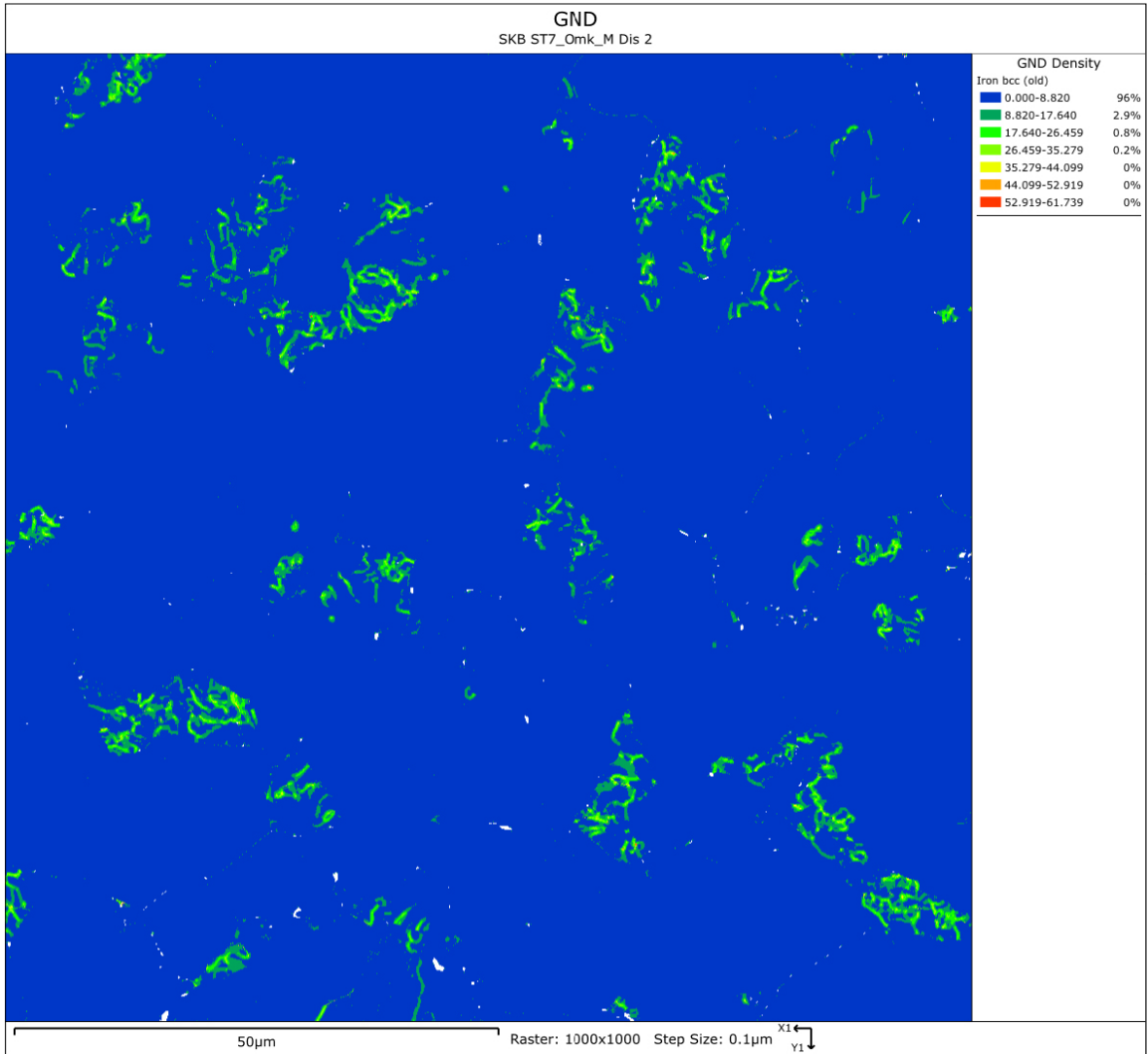


Figure A-20. ST7 circumferential direction, mid position.

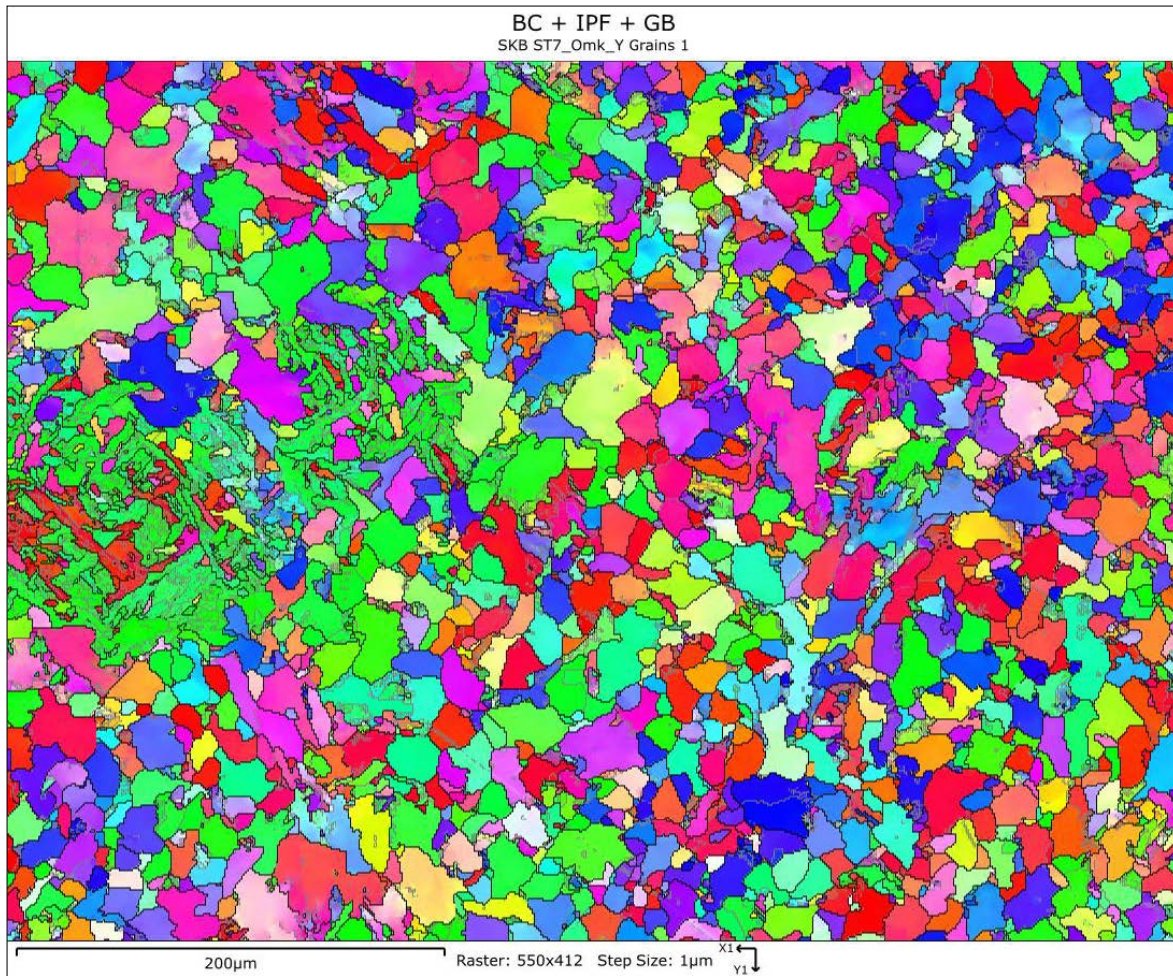


Figure A-21. Specimen ST7 in circumferential direction. Close to outer surface. Lower magnification EBSD analysis showing the grain structure.

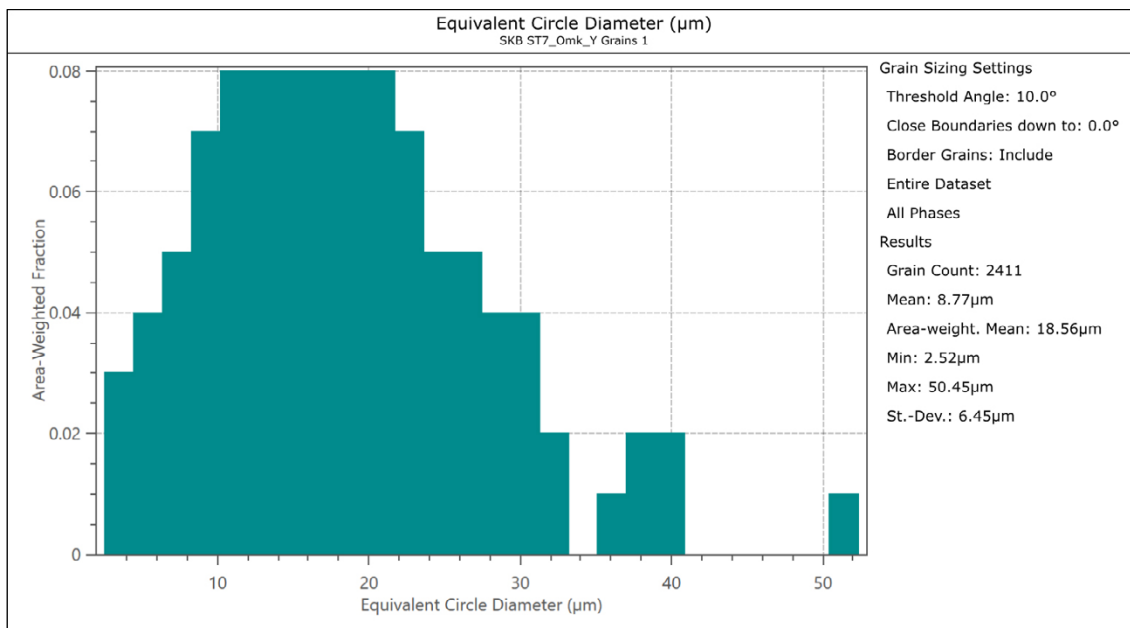


Figure A-22. ST7 circumferential direction, outer surface.

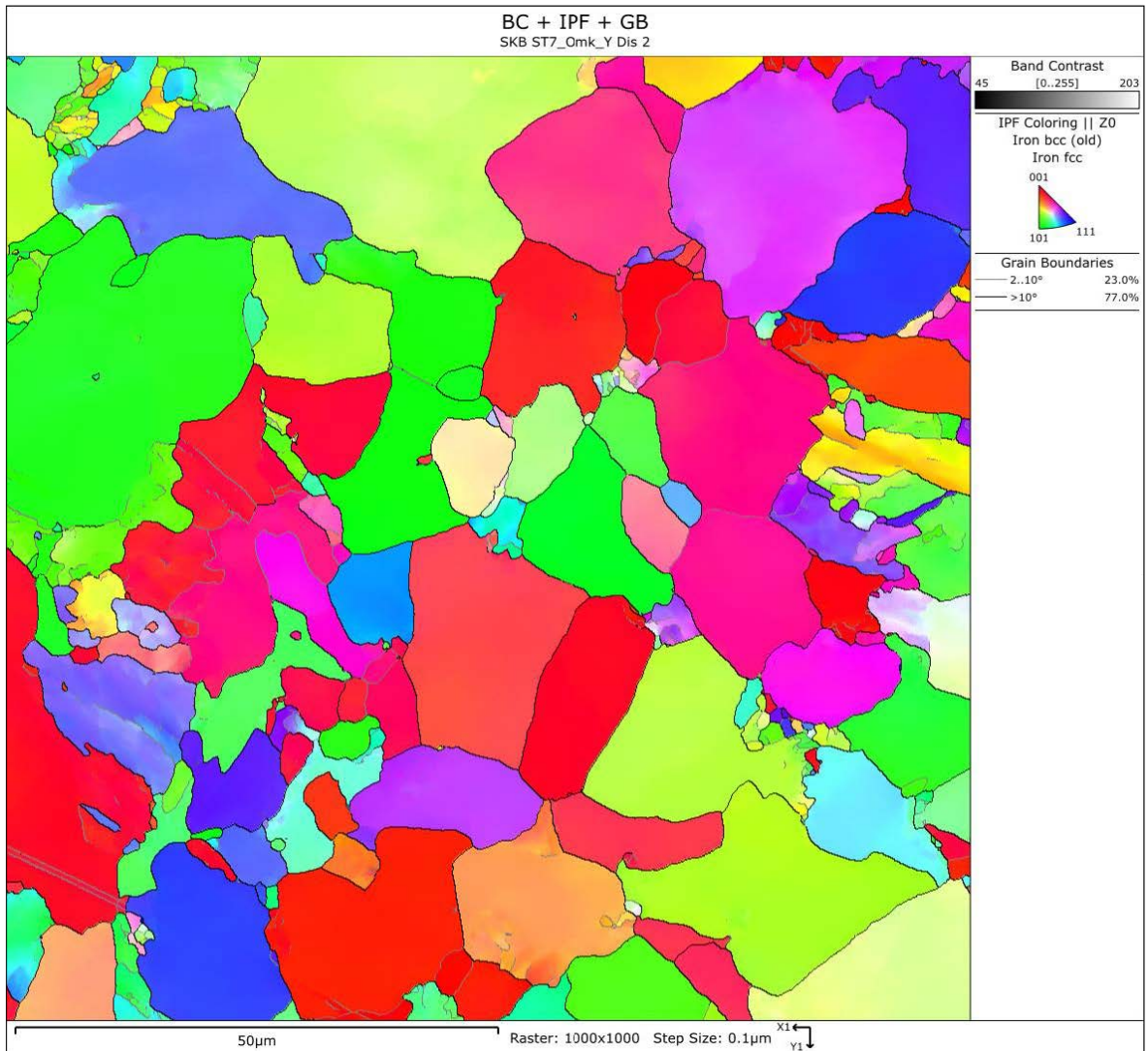


Figure A-23. Specimen ST7 in circumferential direction. Close to outer surface. Higher magnification EBSD analysis for dislocation analysis.

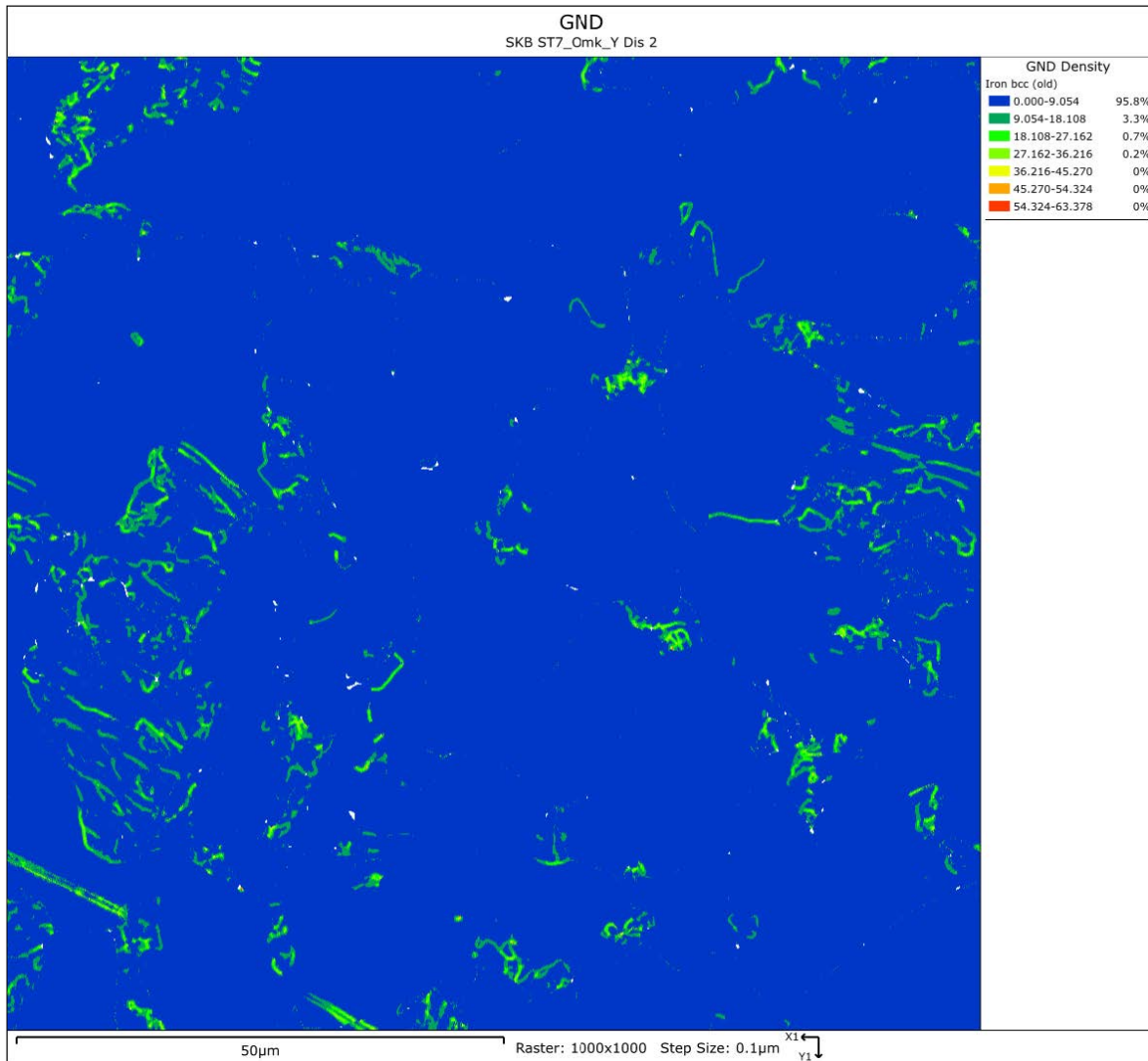


Figure A-24. ST7 circumferential direction, outer surface.

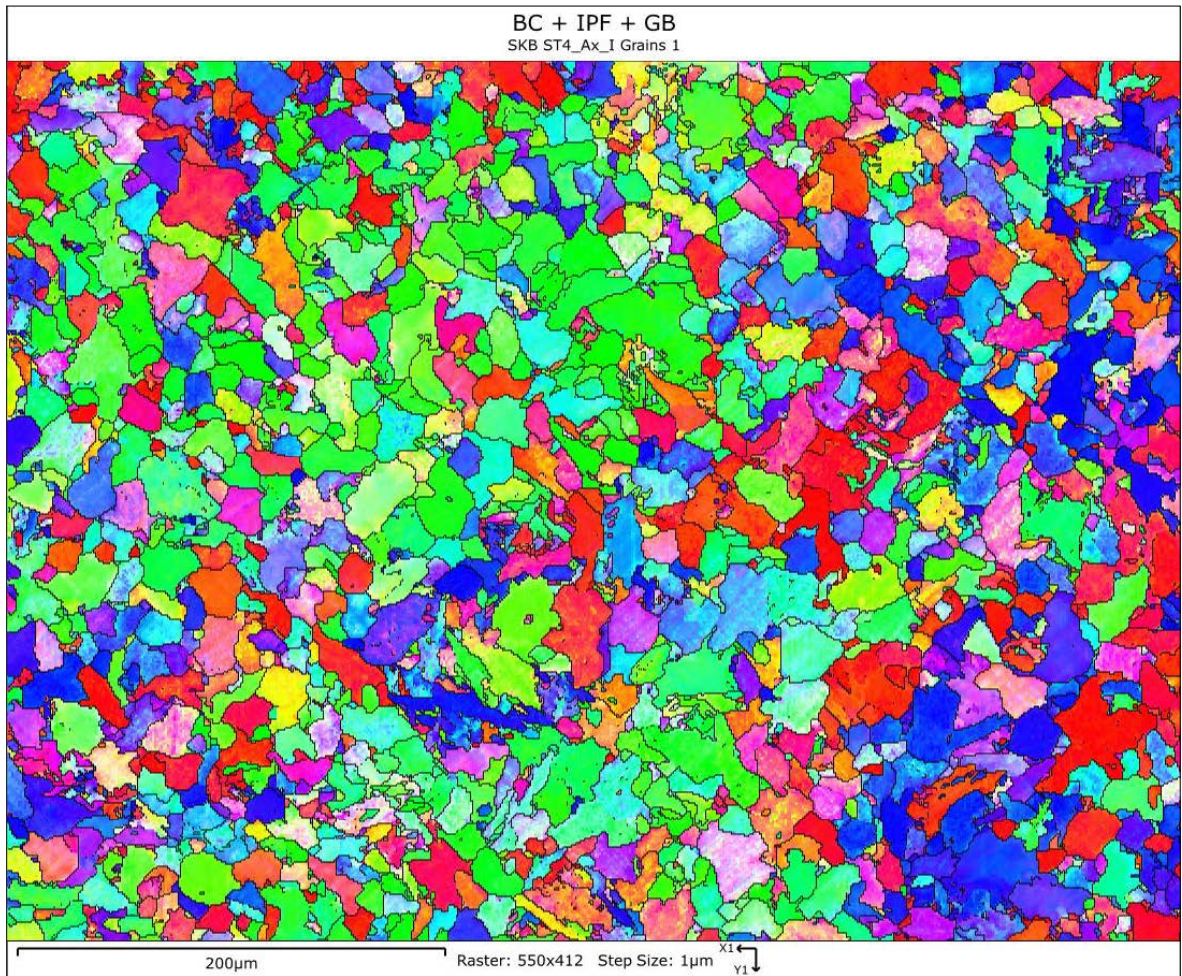


Figure A-25. Specimen ST4 in axial direction. Close to inner surface. Lower magnification EBSD analysis showing the grain structure.

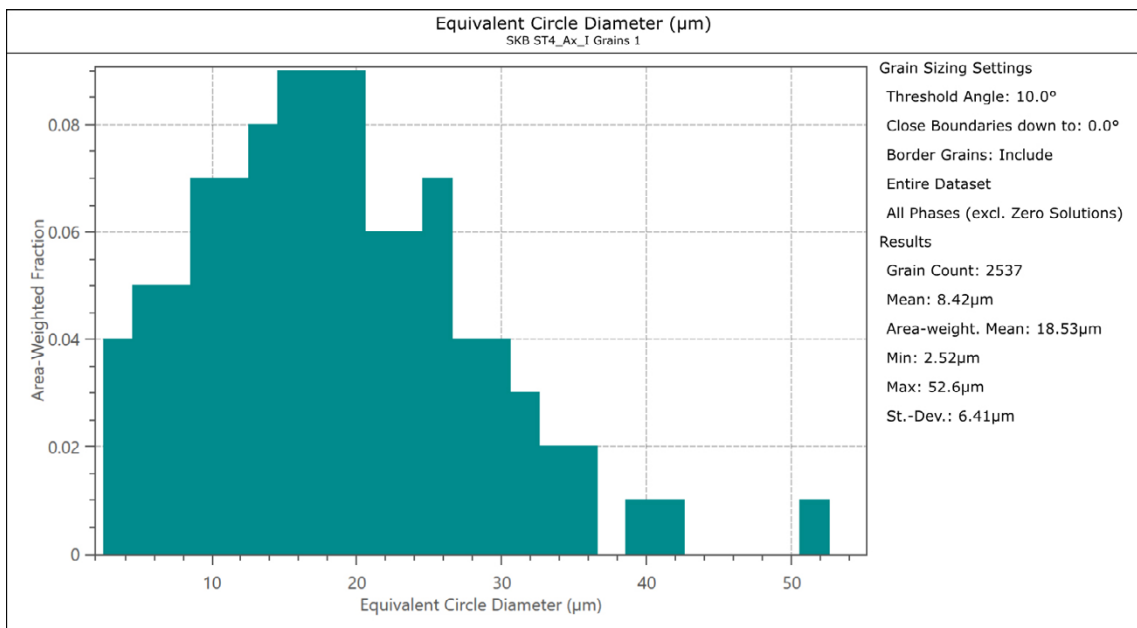


Figure A-26. ST4 axial direction, inner surface.

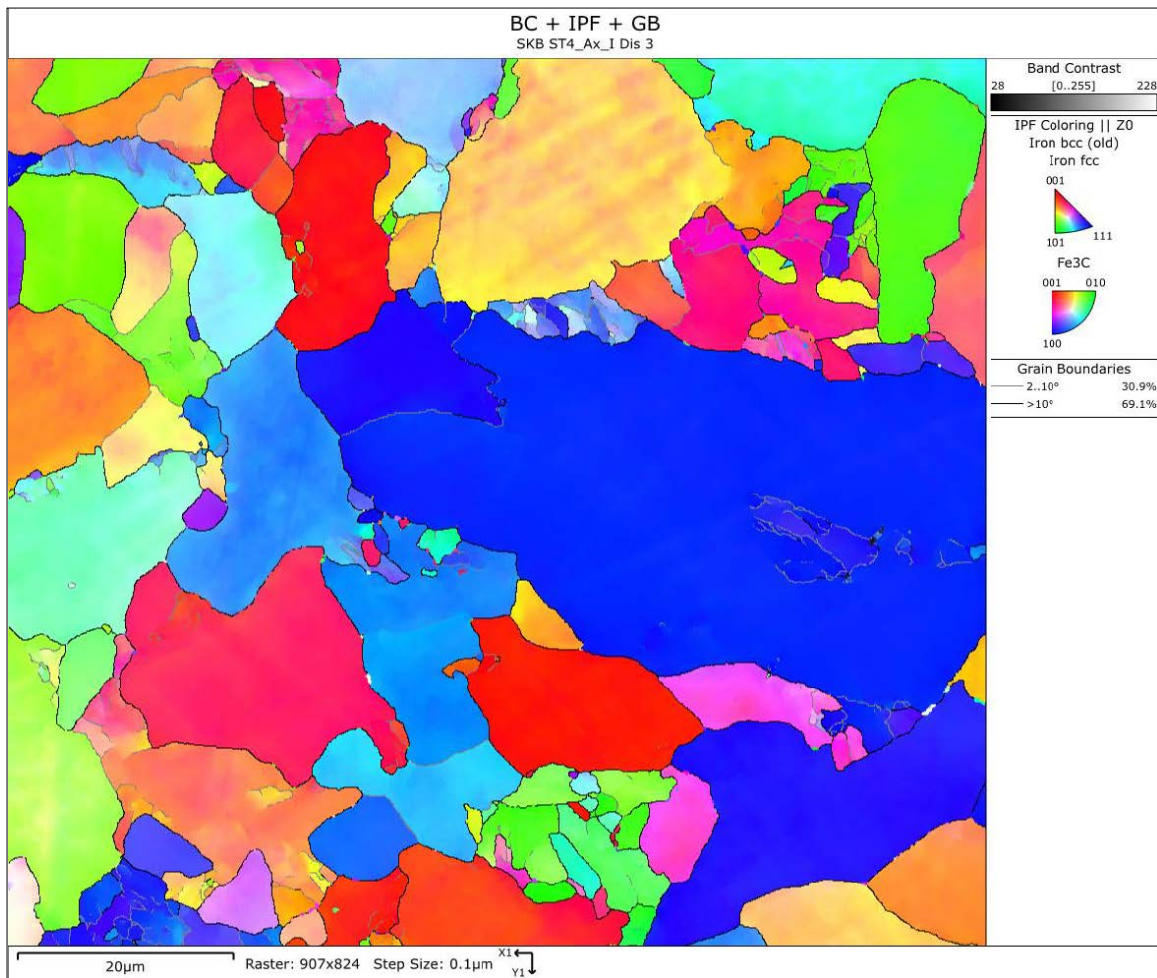


Figure A-27. ST4 axial direction, inner surface.

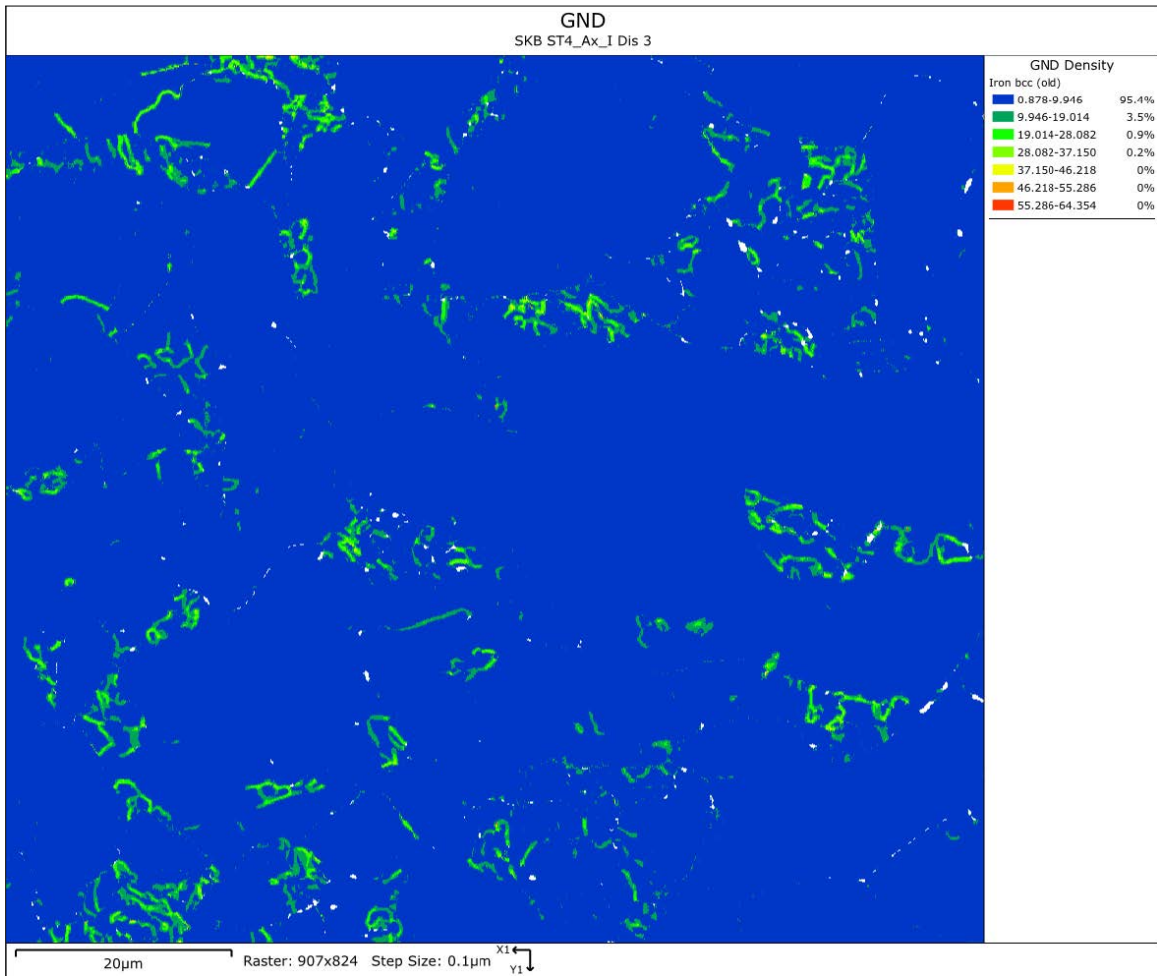


Figure A-28. ST4 axial direction, inner surface.

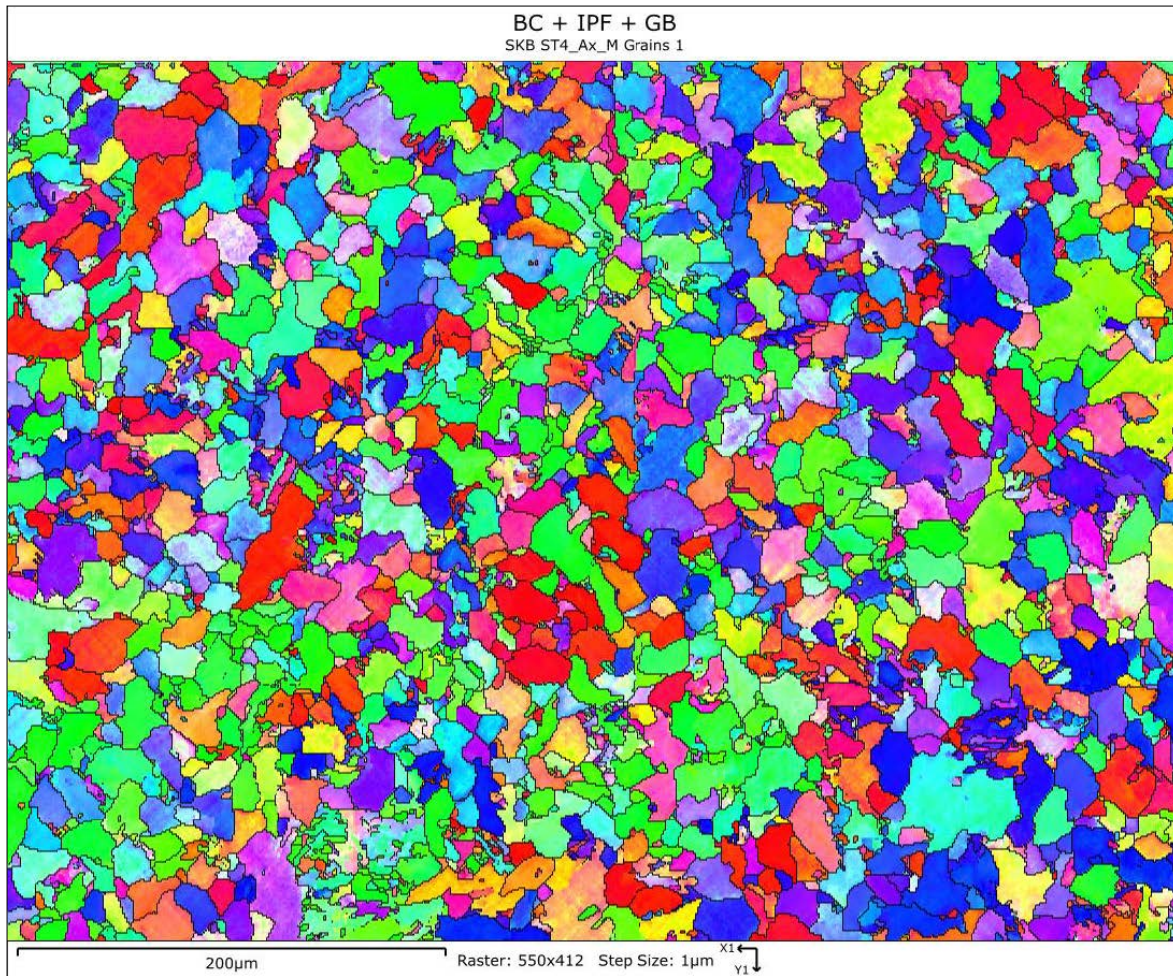


Figure A-29. Specimen ST4 in axial direction. Mid position. Lower magnification EBSD analysis showing the grain structure.

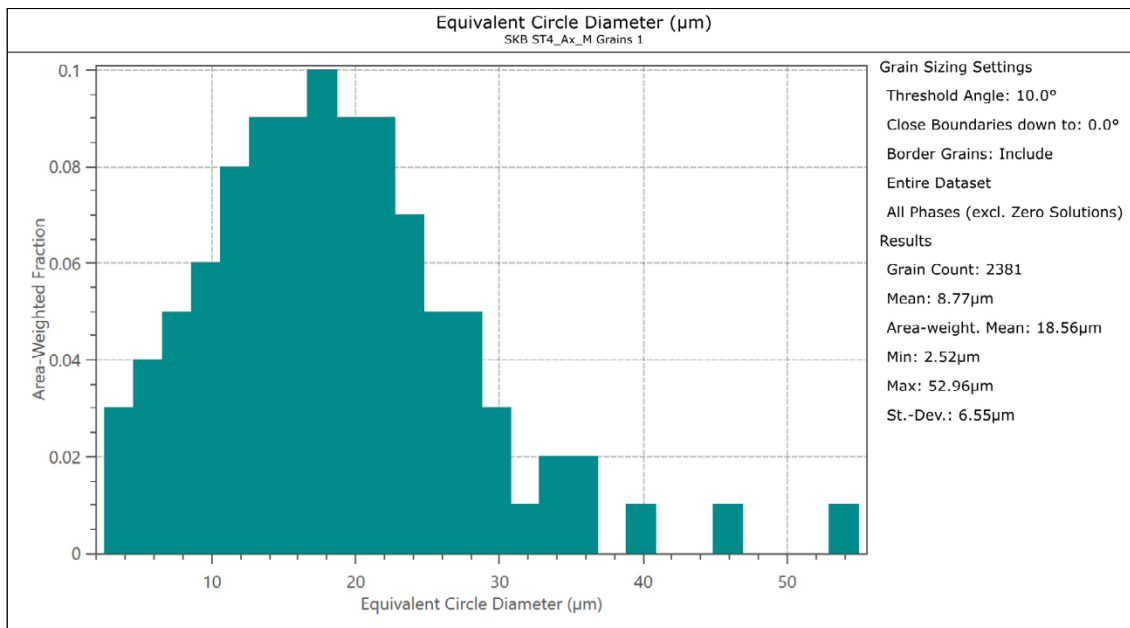


Figure A-30. ST4 axial direction, mid position.

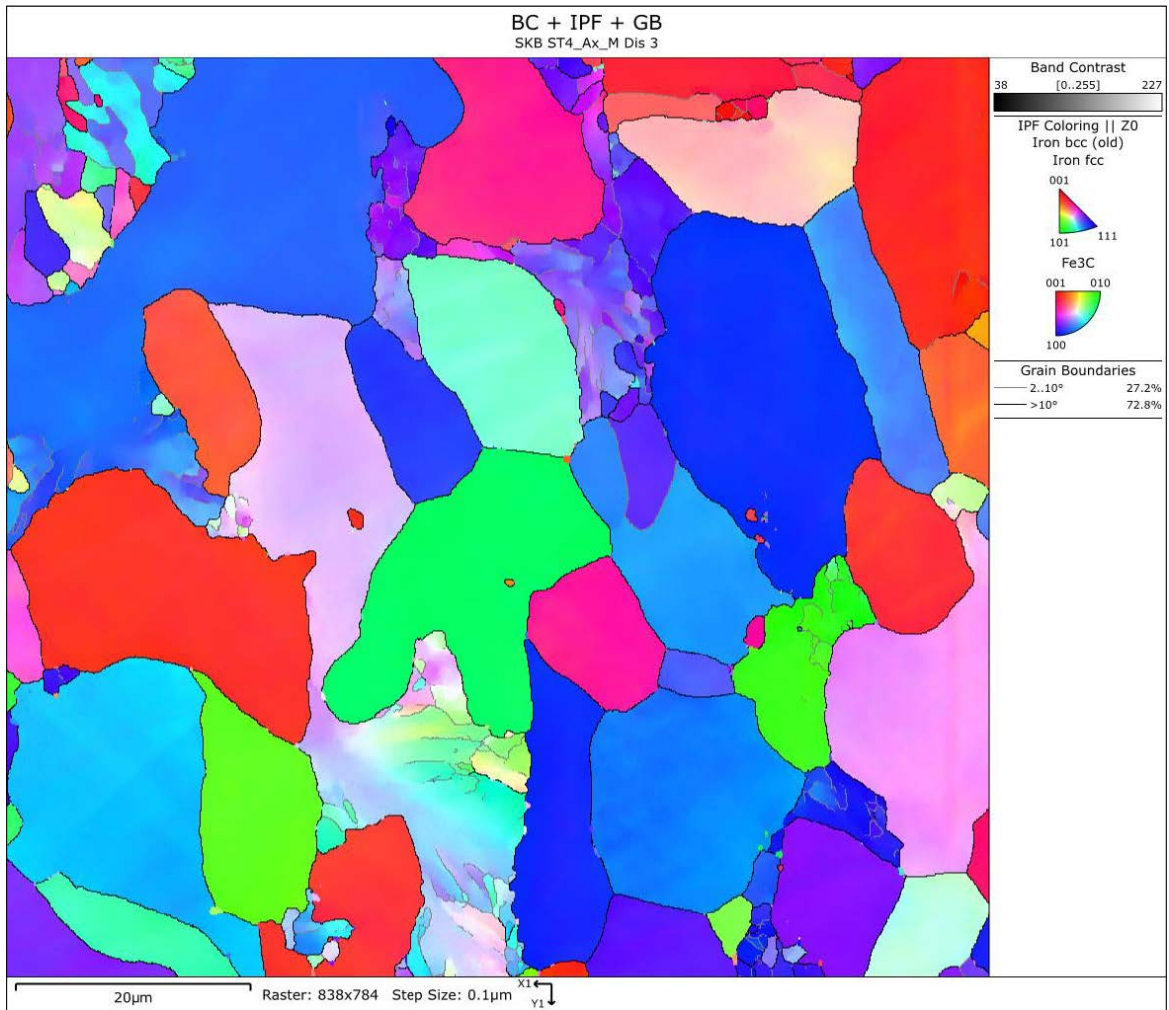


Figure A-31. ST4 axial direction, mid position.

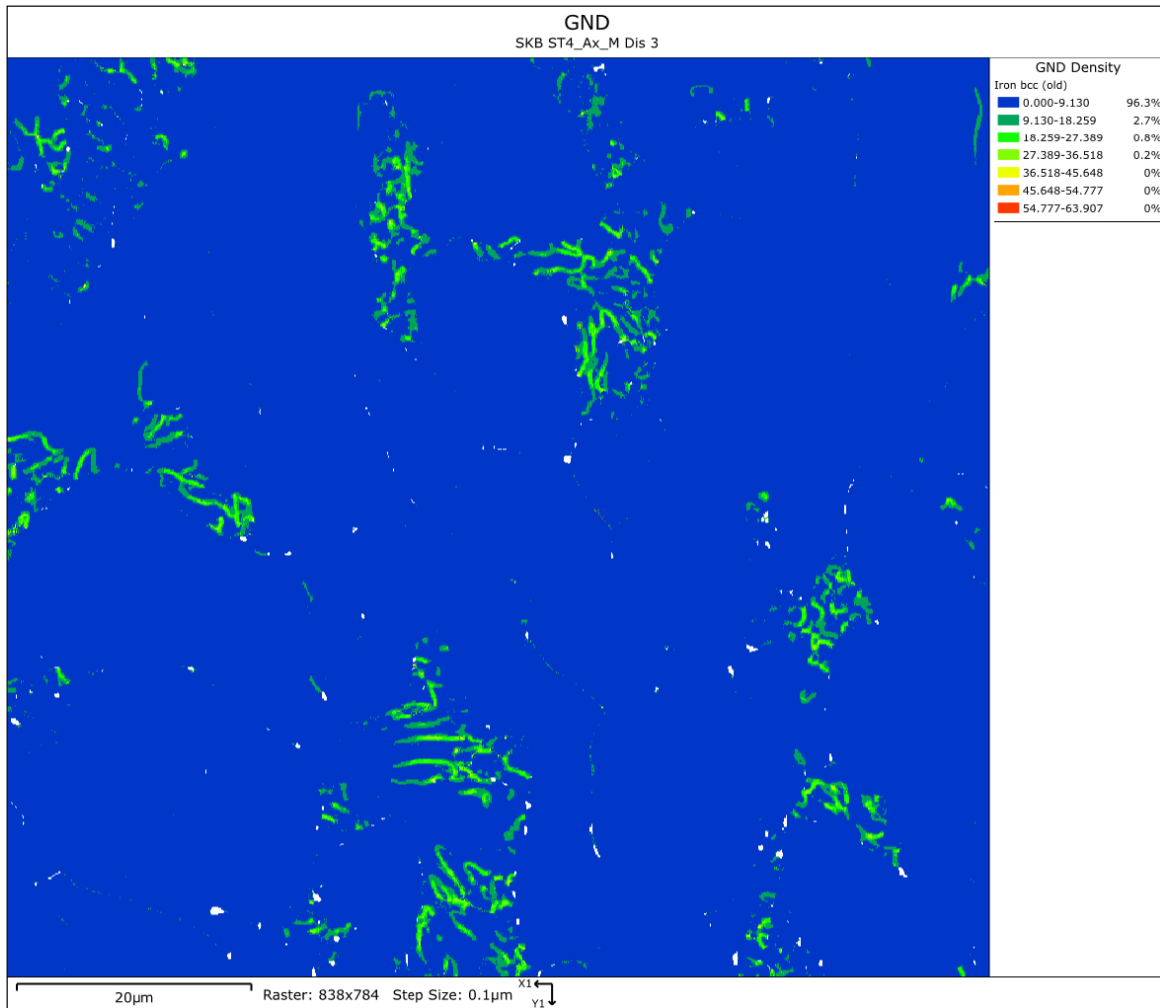


Figure A-32. ST4 axial direction, mid position.

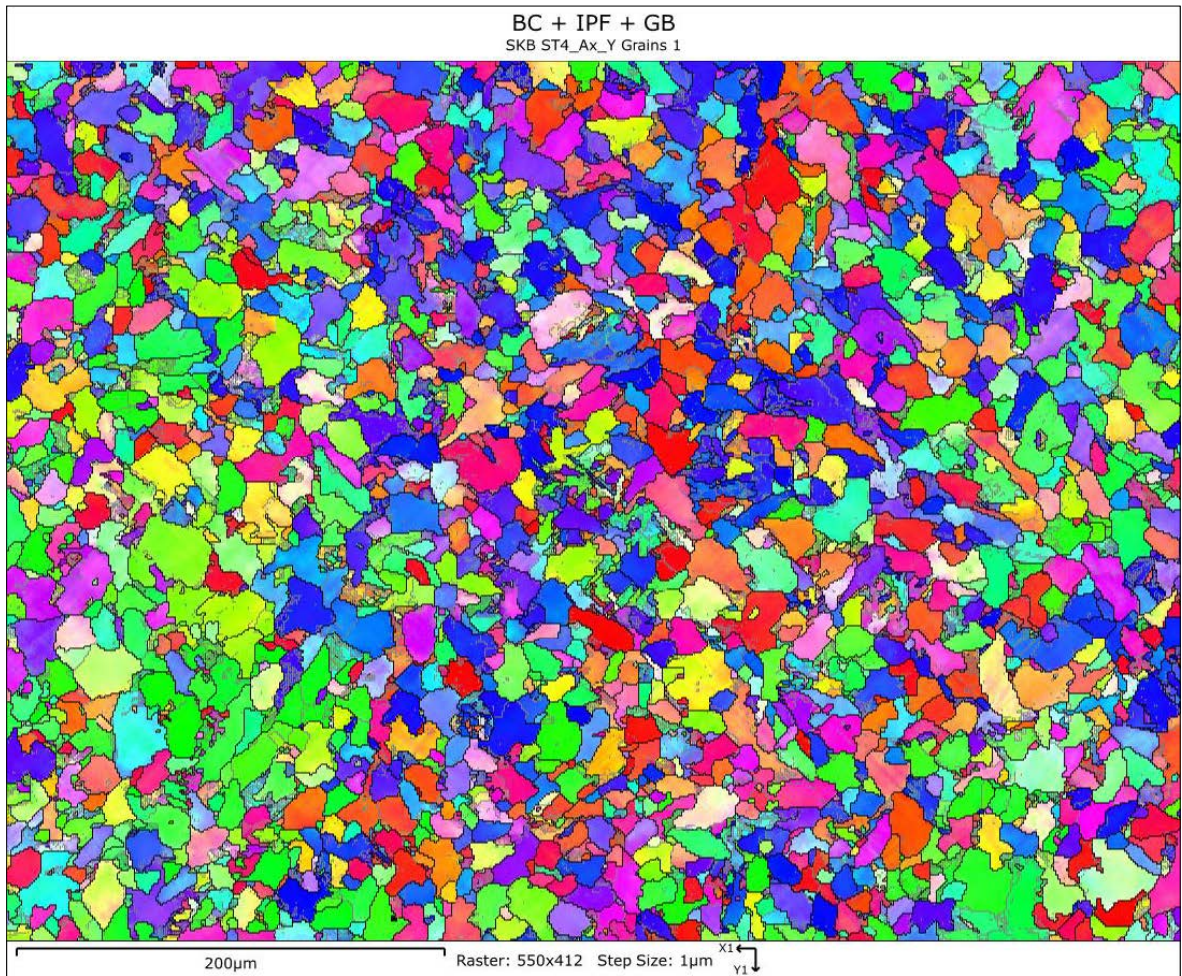


Figure A-33. Specimen ST4 in axial direction. Close to outer surface. Lower magnification EBSD analysis showing the grain structure.

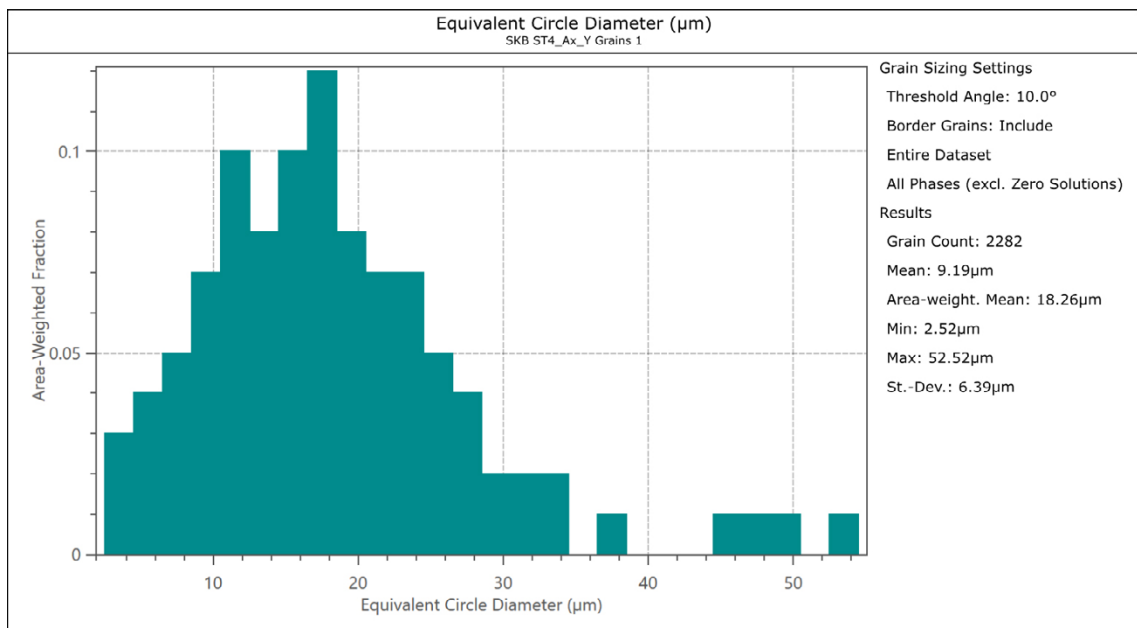


Figure A-34. ST4 axial direction, outer surface.

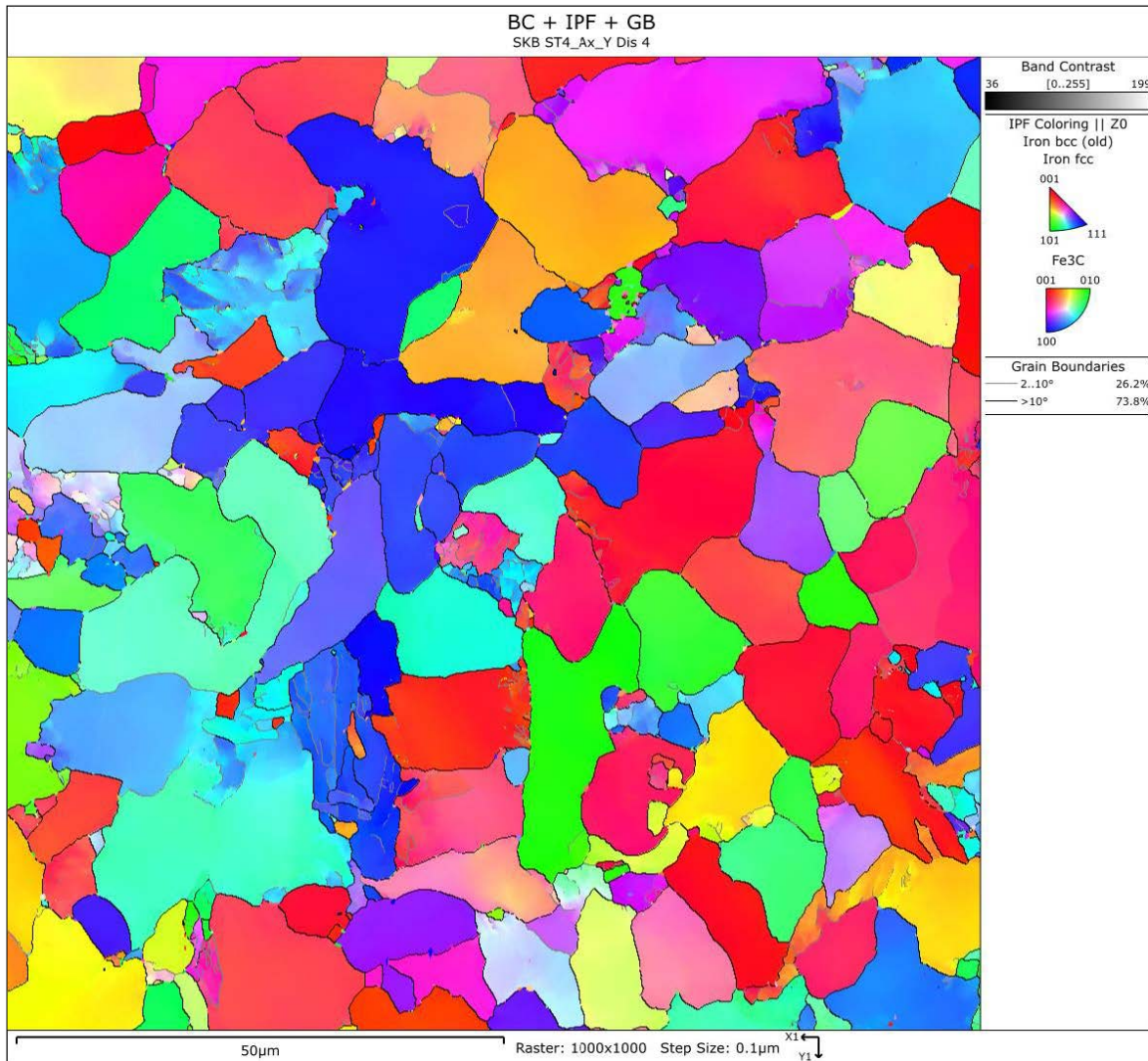


Figure A-35. ST4 axial direction, outer surface.

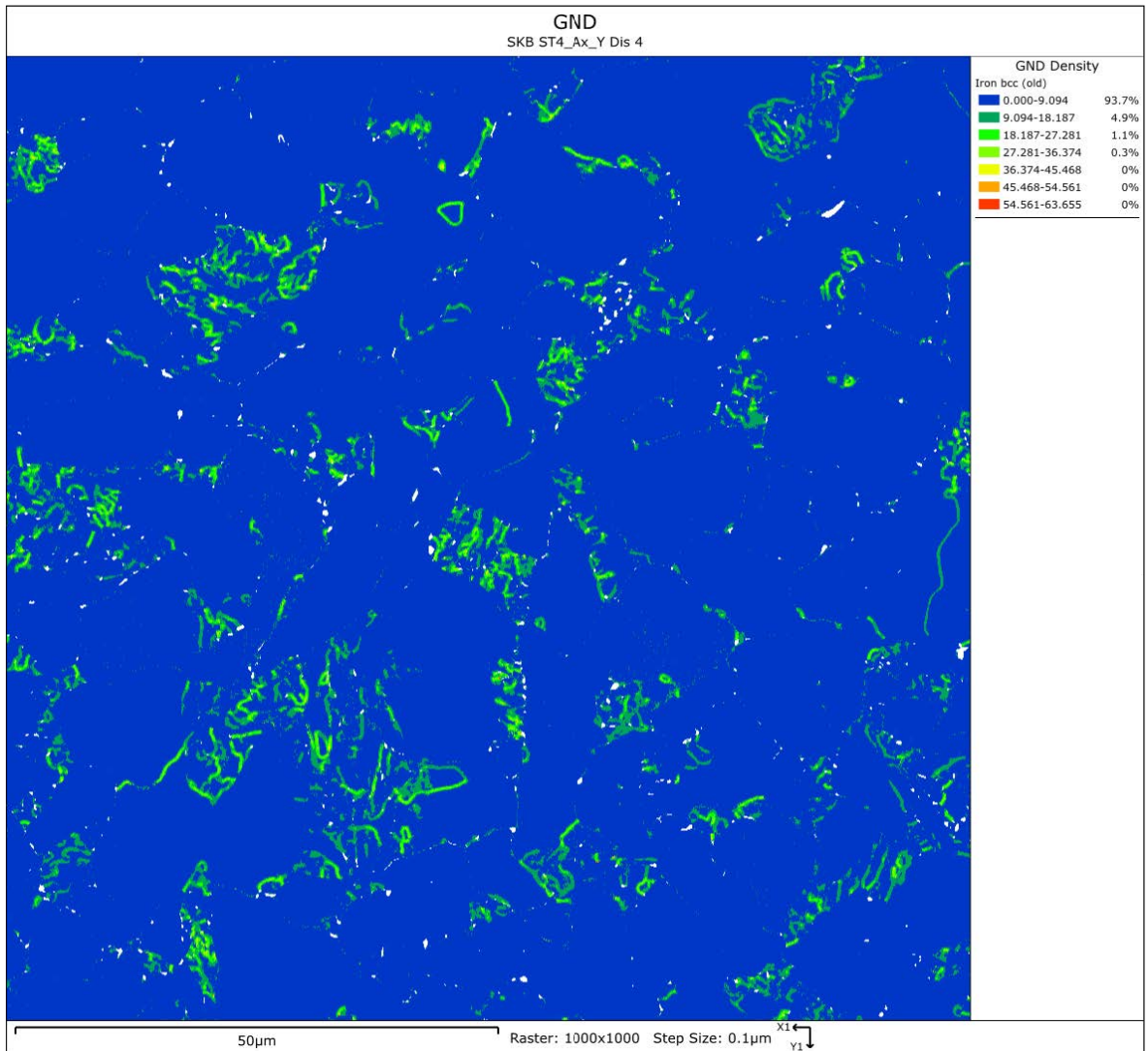


Figure A-36. ST4 axial direction, outer surface.



Figure A-37. Specimen ST4 in circumferential direction. Close to inner surface. Lower magnification EBSD analysis showing the grain structure.

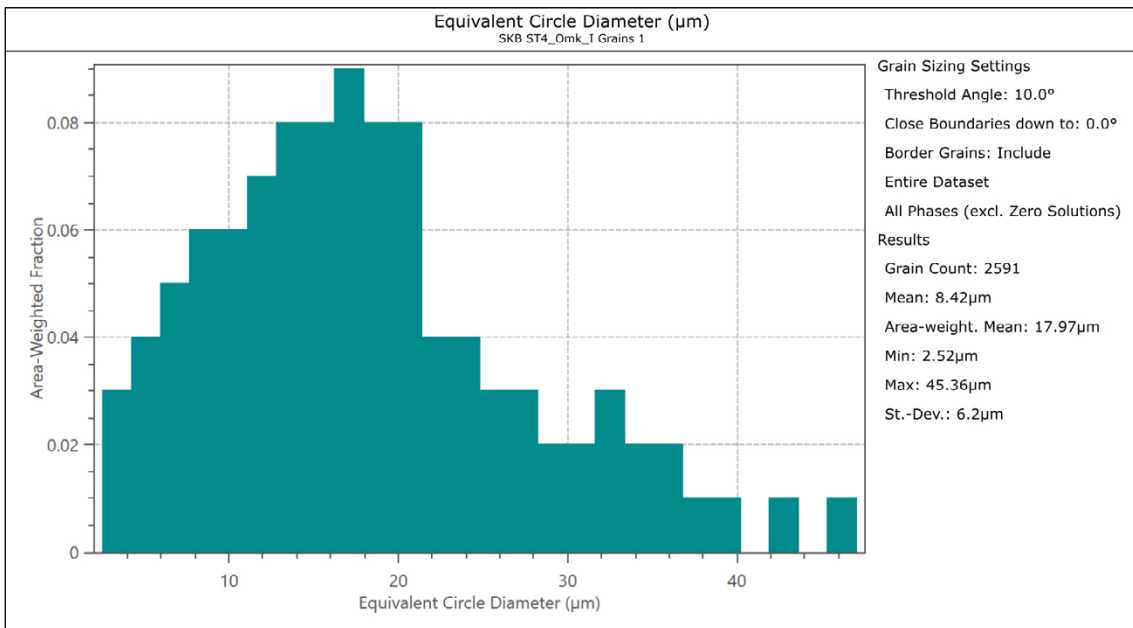


Figure A-38. ST4 circumferential direction, inner surface.

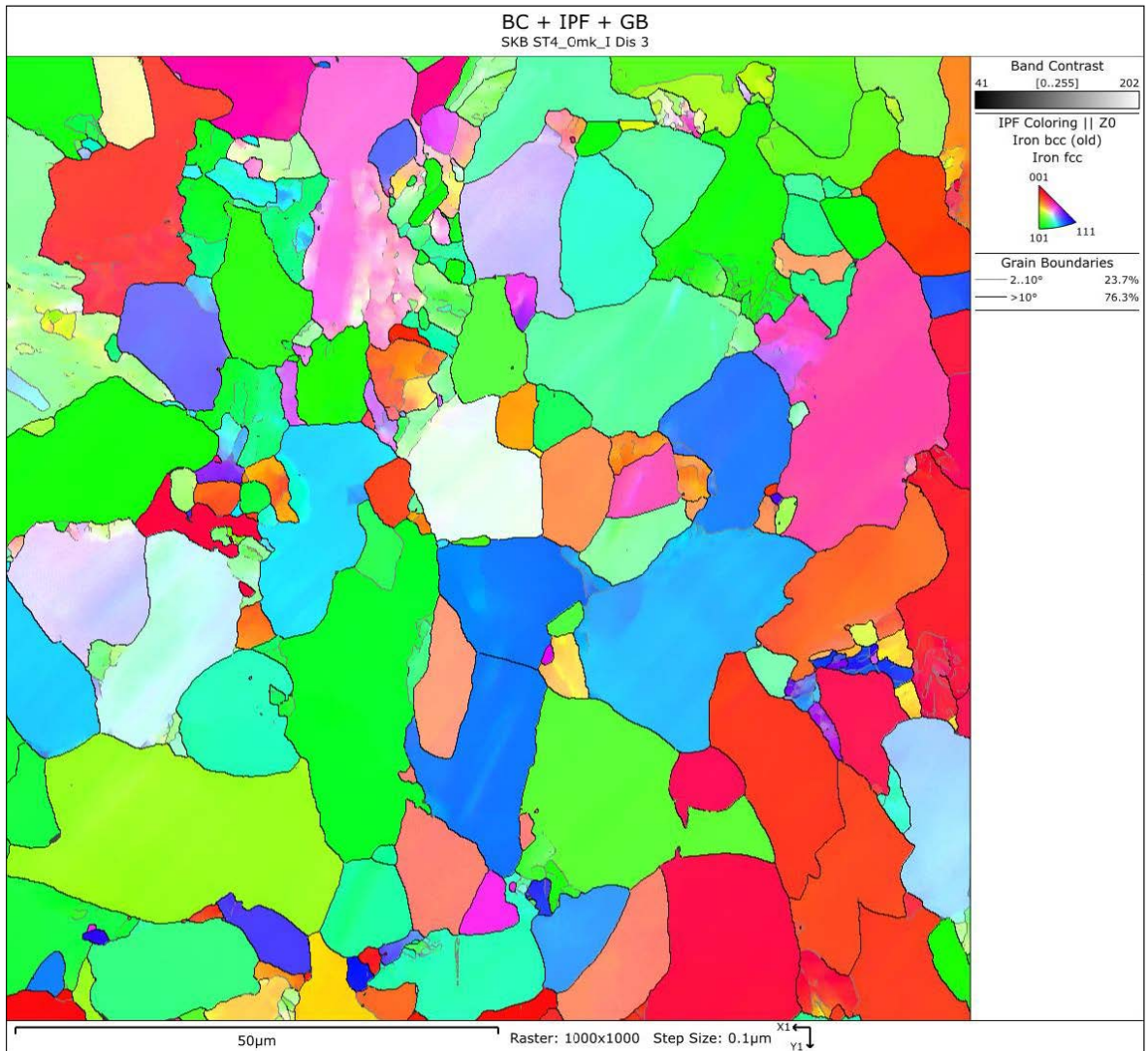


Figure A-39. ST4 circumferential direction, inner surface.

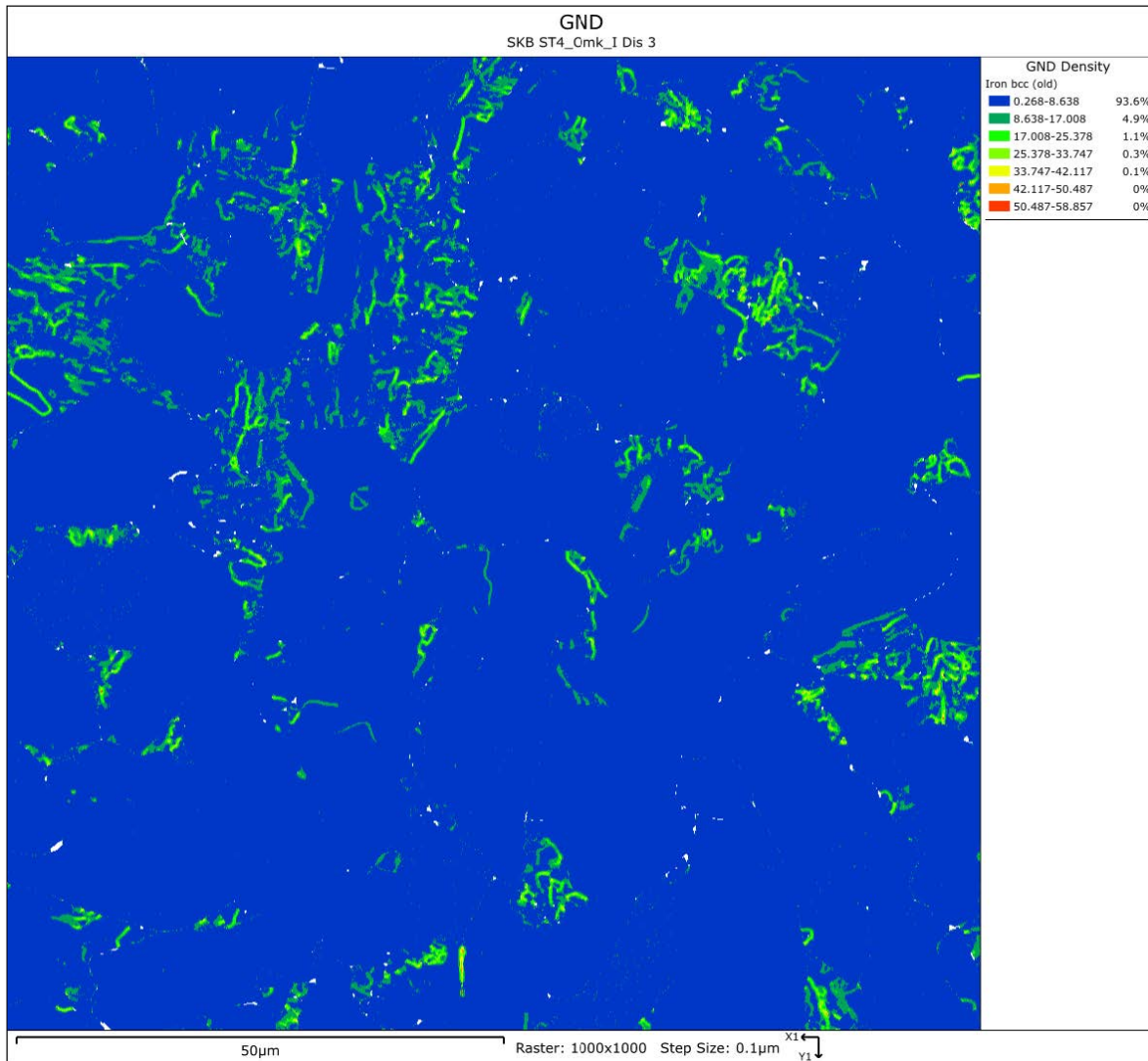


Figure A-40. ST4 circumferential direction, inner surface.

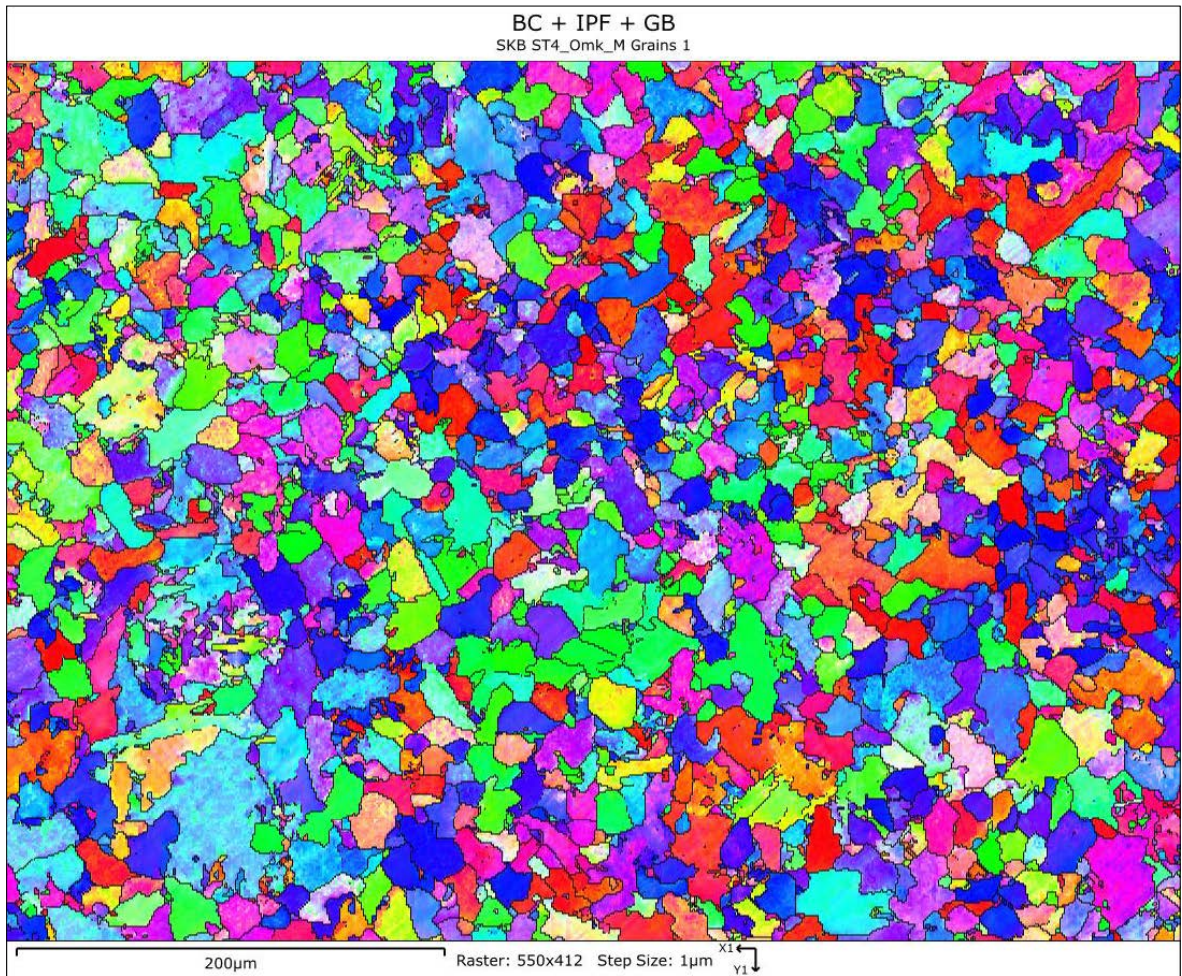


Figure A-41. Specimen ST4 in circumferential direction. Mid position. Lower magnification EBSD analysis showing the grain structure.

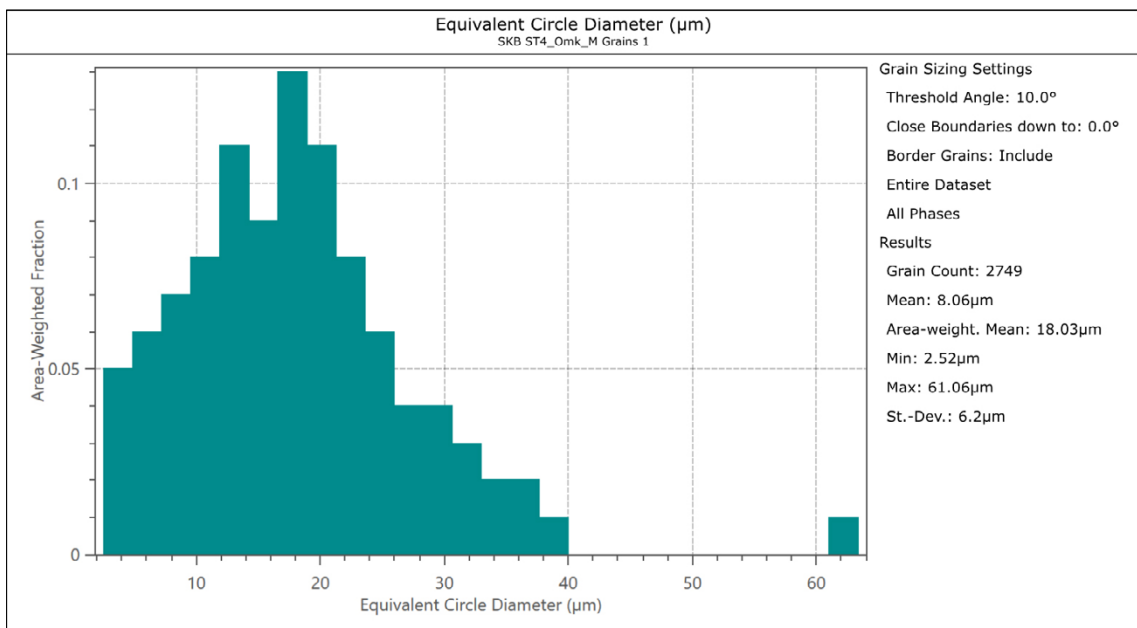


Figure A-42. ST4 circumferential direction, mid position.

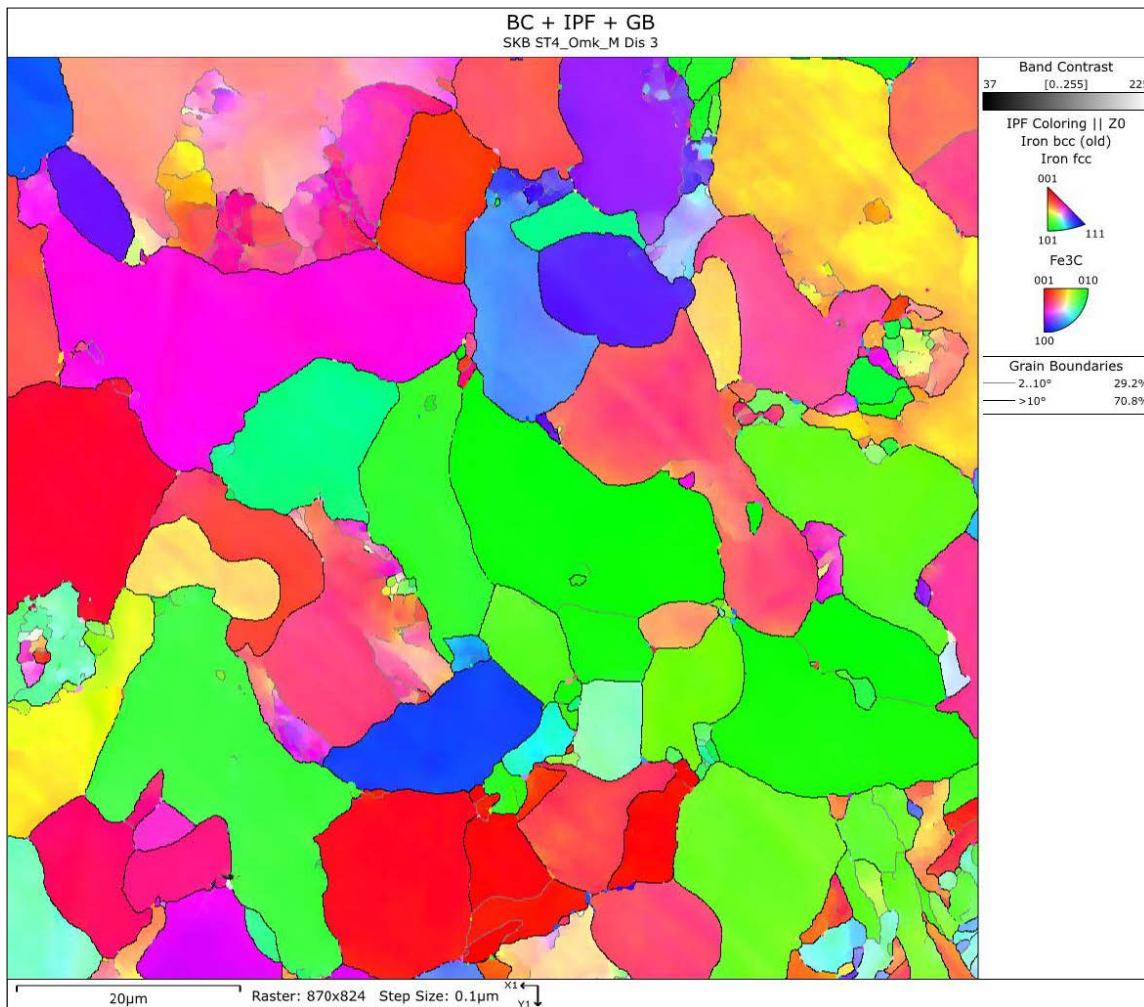


Figure A-43. ST4 circumferential direction, mid position.

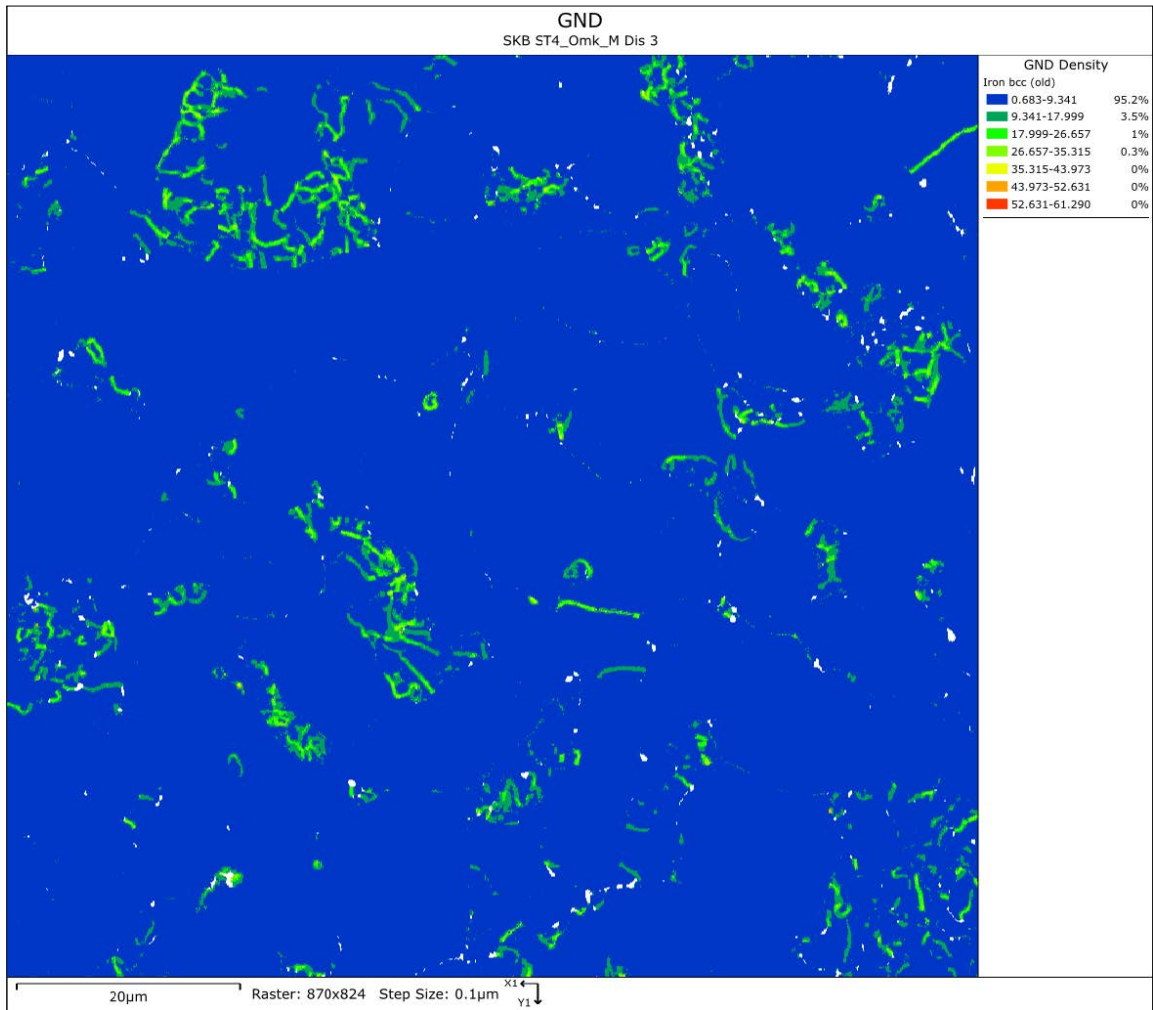


Figure A-44. ST4 circumferential direction, mid position.

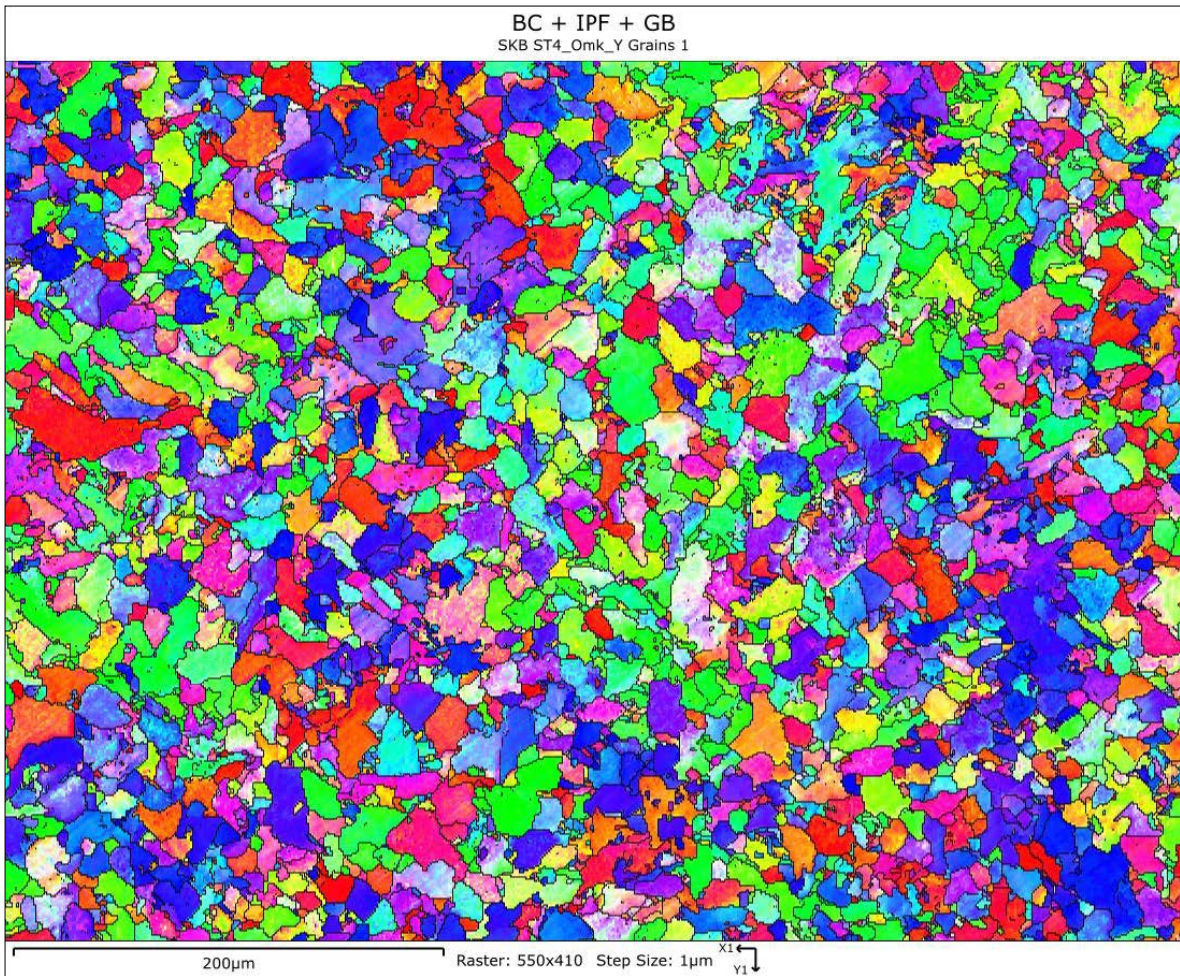


Figure A-45. Specimen ST4 in circumferential direction. Close to outer surface. Lower magnification EBSD analysis showing the grain structure.

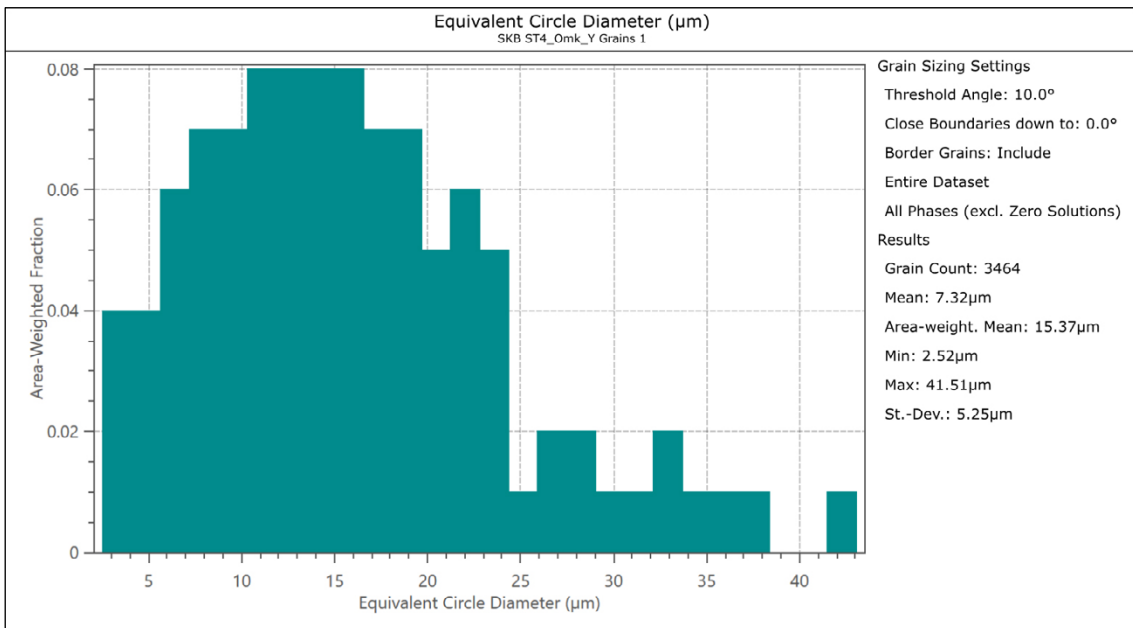


Figure A-46. ST4 circumferential direction, outer surface.

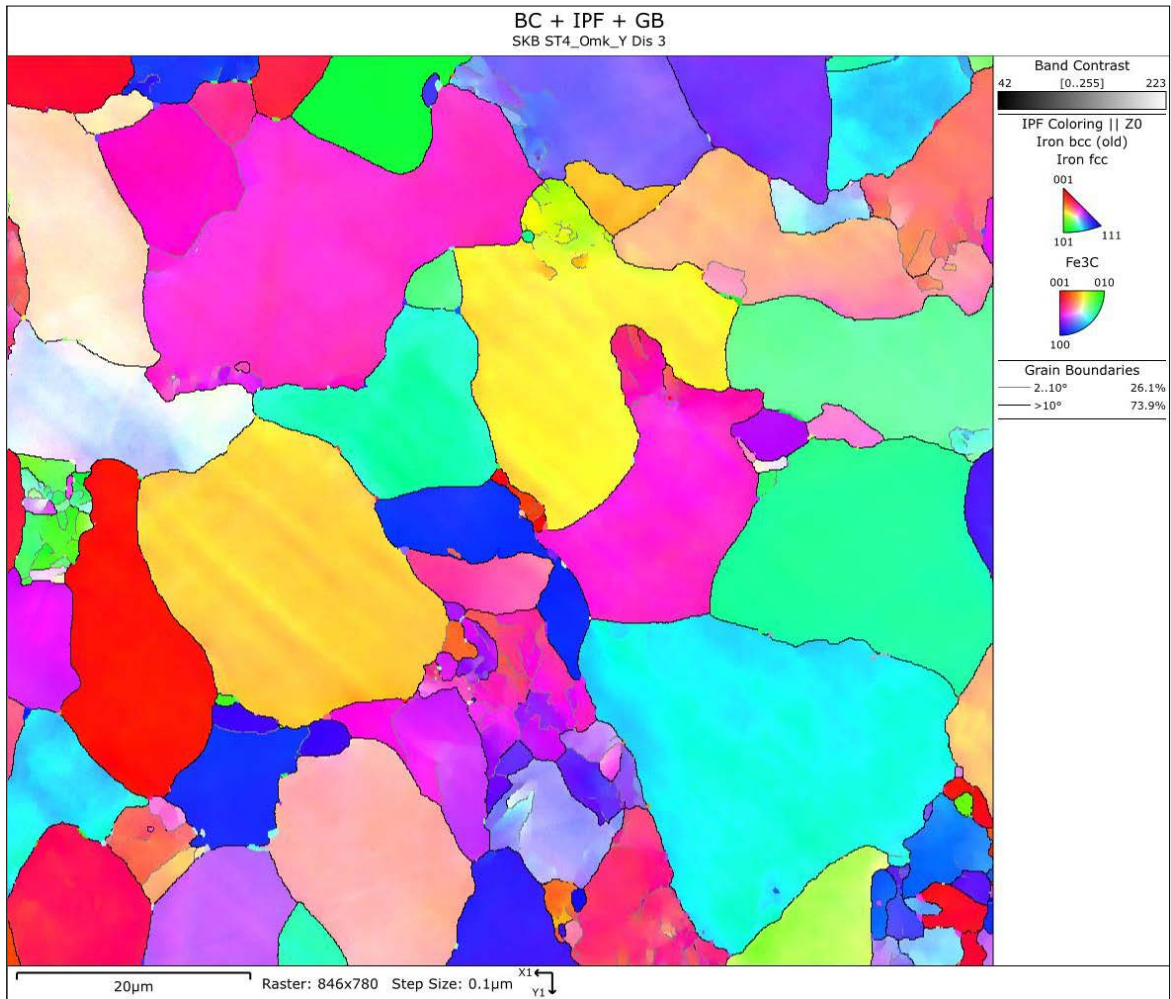


Figure A-47. ST4 circumferential direction, outer surface.

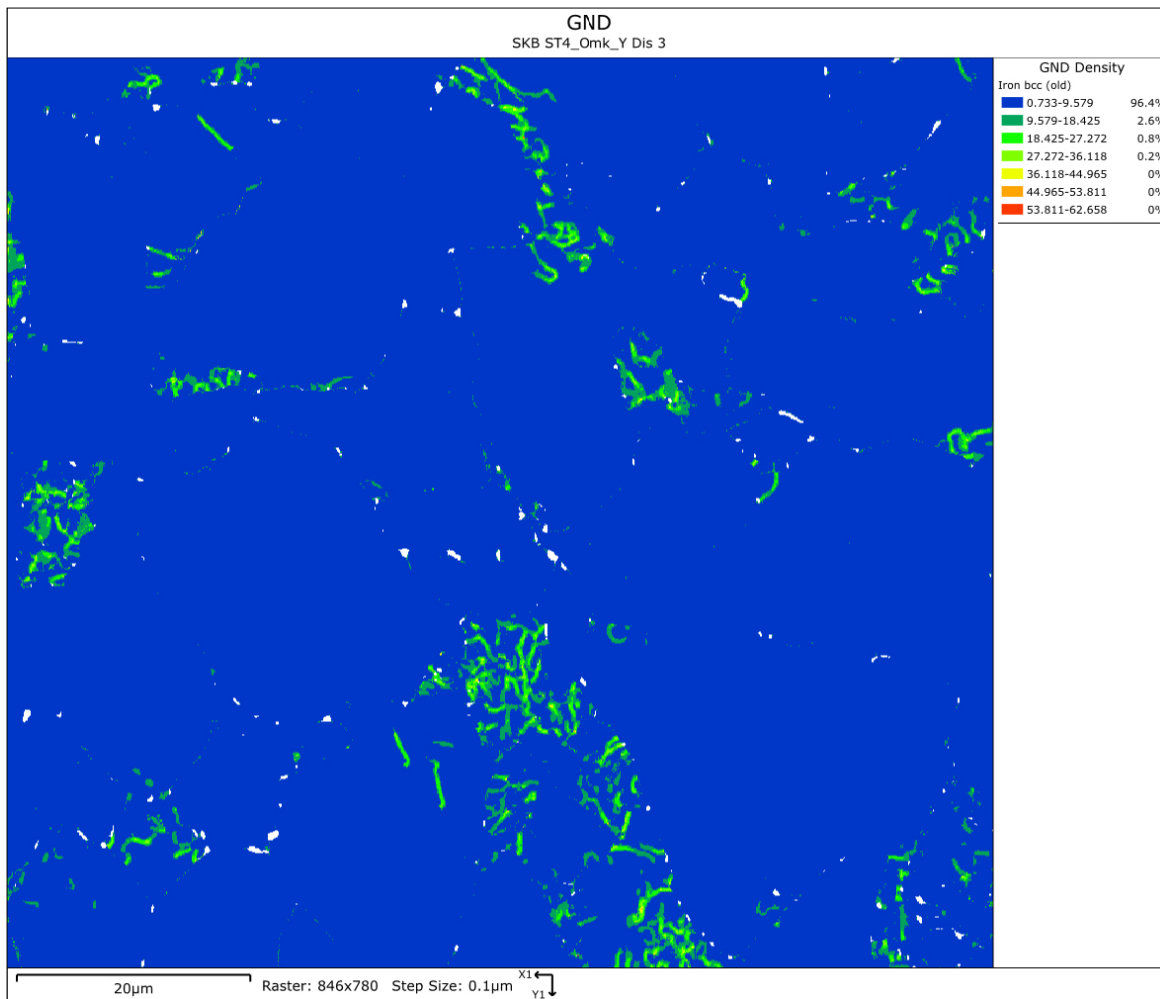


Figure A-48. ST4 circumferential direction, outer surface.

SKB is responsible for managing spent nuclear fuel and radioactive waste produced by the Swedish nuclear power plants such that man and the environment are protected in the near and distant future.

skb.se